DGKε is *S*-palmitoylated at the cysteine located at the cytoplasmic end of its N-terminal transmembrane fragment

Gabriela Traczyk[1], Aneta Hromada-Judycka[1], Anna Świątkowska, Julia Wiśniewska, Katarzyna Kwiatkowska*

[1]equal contribution

Laboratory of Molecular Membrane Biology, Nencki Institute of Experimental Biology PAS, 3 Pasteur St., 02-093 Warsaw, Poland

g.traczyk@nencki.edu.pl

a.hromada-judycka@nencki.edu.pl

a.swiatkowska@nencki.edu.pl

juliawisniewska.work@gmail.com

k.kwiatkowska@nencki.edu.pl

*Corresponding author: Katarzyna Kwiatkowska, Laboratory of Molecular Membrane Biology, Nencki Institute of Experimental Biology PAS, 3 Pasteur St., 02-093 Warsaw, Poland; k.kwiatkowska@nencki.edu.pl

Running title: *S*-palmitoylation of DGKε

Founding sources

This work was supported by the National Science Centre, Poland (grant number 2018/29/B/NZ3/00407).

Abstract

Diacylglycerol kinase-ε (DGKε) catalyzes phosphorylation of diacylglycerol to phosphatidic acid with a unique specificity toward 1-stearoyl-2-arachidonoyl-*sn*-glycerol which is a backbone of phosphatidylinositol (PI). DGKε plays a crucial role in the PI cycle thereby maintaining the cellular level of phosphorylated PI derivatives of signaling activity, and in lipid metabolism. DGKε dysfunction is linked with the development of atypical hemolytic uremic syndrome (aHUS) and other diseases in humans. Despite the DGKε significance, data on the regulation of its functioning by possible co/post-translational modifications are scarce. Here we report that DGKε is *S*-palmitoylated at Cys38/40 (mouse/human DGKε) located at the cytoplasmic end of its N-terminal putative transmembrane fragment. The *S*-palmitoylation of DGKε was revealed by metabolic labeling of cells with a palmitic acid analogue followed by click chemistry, and with acyl-biotin and acyl-PEG exchange assays. The zDHHC7, 17 and 6/16 *S*-acyltransferases were found to catalyze DGKε *S*-palmitoylation which also increased the DGKε abundance, likely by affecting its stability. Given the localization of the majority of DGKε and zDHHC6 in the endoplasmic reticulum and zDHHC7 and zDHHC17 in the Golgi apparatus, trafficking of a fraction of DGKε through the Golgi apparatus toward the plasma membrane is plausible. The Cys38Ala substitution moderately upregulated the activity of DGKε, suggesting an inhibitory effect of the acylation in wild type DGKε. In contrast to Cys38Ala, the substitution of neighboring Pro31 with Ala diminished the amount and the activity of DGKε. Taken together, our data indicate that *S*-palmitoylation can fine-tune DGKε activity and affect its abundance and cellular localization.

Key words: atypical hemolytic uremic syndrome, cell signaling, lipids/chemistry, diacylglycerol kinase, enzymology/enzyme regulation; kinase activity assay, palmitoylation, phosphoinositides, phospholipids/phosphatic acid, zDHHC

Abbreviations:

17ODYA, 17-octadecynoic acid;

aHUS, atypical hemolytic uremic syndrome;

C1, cysteine-rich conserved homology-1;

DAG, diacylglycerol;

HXA, hydroxylamine;

NBD-SAG, 1-NBD-stearoyl-2-arachidonoyl-*sn*-glycerol;

NBD-SAPA, 1-NBD-stearoyl-2-arachidonoyl-*sn*-glycero-3-phosphate;

NBD-PDPA, 1-palmitoyl-2-NBD-dodecanoyl-*sn*-glycero-3-phosphate;

NP-40, Nonidet P-40;

OG, octyl-β-glucoside;

PA, phosphatidic acid;

PI, phosphatidylinositol;

PS, 1,2-diacyl-*sn*-glycero-phosphoserine;

SAG, 1-stearoyl-2-arachidonoyl-*sn*-glycerol or 18:0/20:4-DAG;

TCEP, Tris(2-carboxyethyl)phosphine hydrochloride;

TLC, thin layer chromatography;

zDHHC, zinc finger DHHC domain containing

INTRODUCTION

Diacylglycerol kinases (DGK) catalyze phosphorylation of DAG to phosphatidic acid. Ten mammalian DGKs, isoenzymes α-κ, have been identified and classified into five groups depending on their structure. They all contain two (or three) cysteine-rich conserved homology-1 (C1)-like domains and a catalytic and an accessory domain but their regulatory domains differ (1,2). DGKε is unique among them - it lacks regulatory domains and is thought to be incorporated into a membrane by a hydrophobic fragment comprising 21 amino acids near its N-terminus (residues 22-42 in human hDGKε, and 20-40 in mouse mDGKε) that is highly conserved in vertebrates (3, 4). DGKε is also distinguished from other DGKs by its specificity toward DAG bearing C16:0 or C18:0 and 20:4 fatty acids at the *sn*-1 and *sn*-2 position, respectively (5-8). The C18:0/20:4 DAG (SAG) is the backbone of phosphatidylinositol (PI) and its phosphorylated derivatives, therefore DGKε activity contributes to the so-called PI cycle (9). This enzymatic cycle serves to rebuild the cellular PI pool following the hydrolysis of PI(4,5)P_2 in the course of signal transduction by a large number of plasma membrane receptors. The interest in DGKε is further enhanced by the link detected in mouse models between its activity and the development of Huntington's disease, seizure susceptibility, and protection from obesity (10-12). Importantly, mutations of *DGKE* are linked with the atypical hemolytic uremic syndrome (aHUS) in humans (13; see https://bibliome.ai/hg19/gene/DGKE for current update). Some of those abnormalities have been correlated with changes in PI(4,5)P_2 turnover (10, 14).

These features make DGKε of significant interest but the complexity of its regulatory mechanisms is only beginning to be elucidated. Thus, although DGKε contains the C1A and C1B domains resembling those which bind DAG in conventional and novel protein kinase C isoforms, SAG binds to the lipoxygenase (LOX)-like motif of DGKε rather than to those domains (15, 16). On the other hand, the C1 domains can interact with the catalytic domain of DGKε (4, 17) and co-determine its substrate specificity, in analogy to DGKα (8). Our group found recently that the activity and stability of DGKε depend on the zinc finger motif present in the C1B domain. Substitution of any of the cysteines and the histidine of this motif, notably found in some aHUS patients, inactivates the kinase and leads to its proteasomal degradation (18). Finally, the

activity and substrate specificity of DGKε are up-regulated allosterically by membrane morphology, i.e., by negatively curved membranes (19). The latter suggests that DGKε functioning can depend on its localization in specific regions of cellular membranes.

S-palmitoylation is one of the factors that contribute to the accumulation of proteins, both transmembrane and peripheral ones, in selected domains of cellular membranes, including membranes of the endoplasmic reticulum, Golgi apparatus, and the plasma membrane (20-24). This posttranslational modification consists in the attachment of a palmitic acid residue to the sulfhydryl group of cysteine via a thioester bond and is potentially reversible. It is catalyzed by *S*-acyltransferases from the zinc finger DHHC domain containing (zDHHC) family, of 23 enzymes in mammals (25-27). We have recently discovered that DGKε is palmitoylated and the amount of such modified protein increases in Raw264 macrophage-like cells after LPS stimulation (28). It has been established that proteins can be acylated with fatty acids other than palmitic acid, and on rare occasions, the acyl chain can be attached to amino acids other than cysteine (29). Therefore, drawing on recent methodological progress in this work we continued studies on DGKε acylation. The click chemistry-based technique requires metabolic labeling of cells with a fatty acid analogue bearing an alkyne (or azide) moiety at the omega carbon. After cell lysis, the acylated proteins are detected by a "click" reaction between the alkyne (or azide) and an azide (or alkyne) residue of a reporter tag, either biotin or a fluorescent dye. This technique does not discriminate between *S*-acylation of cysteine and the rare *O*- and ε-*N*-acylation at serine or threonine and lysine, respectively (30, 31). On the other hand, the acyl-biotin exchange (ABE) technique relies on the substitution of a thiol-bound fatty acid with a thiol-reactive biotin derivative, hence it only detects *S*-acylation, including *S*-palmitoylation (32). However, it can give false-positive results by detecting proteins forming a thioester linkage with moieties other than fatty acids, like some enzymes of the ubiquitination cascade forming thioester intermediates with ubiquitin (33).

Taking into account the pros and cons of the click-based chemistry and ABE we used both these techniques to study the *S*-palmitoylation of DGKε and identified Cys38/40 (mouse DGKε/human DGKε) as the site of this modification. We also found that DGKε can be *S*-palmitoylated by zDHHC6/16, zDHHC7

and zDHHC17 and that this modification increased the steady-state mDGKE level, likely by affecting its stability, and can also moderately down-regulate DGKε activity.

MATERIALS AND METHODS

Plasmids

cDNA of mouse DGKε (mDGKε, NM_019505) was obtained and cloned into the pcDNA3.1/Hygro(+) vector (Invitrogen) and fused with a double Myc tag at the C-terminus, as described by Traczyk et al. (18). Plasmid encoding human DGKε (hDGKε, NM_003647) was purchased from OriGene (cat. No. RC219913). The *DGKE* coding sequence was subcloned into the pcDNA3.1/Hygro(+)-2xMyc vector using primers: forward 5'-CTTTCTAGAACCATGGAAGCGGAGAGGCG-3' and reverse 5'-CTTTCTAGATTCAGTCGCCTTTATATCTTCTTGA-3' and XbaI restriction enzyme to obtain hGDKε doubly Myc-tagged at the C-terminus. DGKε mutant forms were prepared by site-directed mutagenesis; all wild type and mutant DGKε-Myc constructs were verified by sequencing (Genomed SA). Primers used for *Dgke* and *DGKE* mutagenesis are listed in Supplemental Table S1. A library of pEF-BOS-HA plasmids encoding HA-tagged mouse DHHC1 - DHHC23 *S*-acyltransferases and GST for control were obtained from Prof. Masaki Fukata (National Institute of Physiological Sciences, Okazaki, Japan; 25, 34).

Cell culture and transfection

HEK293 cells (ATCC CRL-1573™, mycoplasma-free) were plated at $1.2 \cdot 10^6$ in a 6-cm dish (for click, ABE and APE) or $0.5 \cdot 10^5$ in a 3.5-cm dish (for activity measurements). After 24 h, the cells were transfected with 2 µg (for click and ABE in experiments with no ectopic expression of *S*-acyltransferases) or 850 ng (for activity measurements) of pcDNA3.1/Hygro(+) plasmids encoding wild type mDGKε or hDGKε or their mutants using 8 µl or 3.4 µl FuGENE HD (Promega) in 3.3 ml or 1.5 ml DMEM containing 4.5 g/l glucose and 10% FBS, according to the manufacturer's instruction. To identify the zDHHC *S*-palmitoylating DGKε, cells ($1.2 \cdot 10^6$ in a 6-cm dish) were transfected with 1 µg (ABE) or 2 µg (APE) of pcDNA3.1/Hygro(+) plasmid encoding wild type mDGKε-Myc together with 1 µg (ABE) or 2 µg (APE) of pEF-BOS-HA plasmid bearing one of the 23 *Zdhhc* genes or *Gst* using 8 or 16 µl FuGENE HD in 3.3 ml DMEM/glucose/FBS, as above. In a series of experiments, pcDNA-mDGKε-Myc was co-transfected with pEF-BOS-HA plasmids encoding DHH6 and DHHC16 (1 µg each/dish). Also, when indicated the plasmids

encoding mDGKε-Myc or DHHC-HA were substituted with respective amounts of empty pcDNA3.1 Hygro(+) vector. After 24 h (identification of zDHHC *S*-palmitoylating DGKε according to Fukata et al., 34) or 48 h, the cells were harvested in cold PBS, pelleted and stored at -80°C. For click and activity measurements the culture medium was exchanged after 24 h for DMEM containing glucose and FBS as above with 0.05 mg/ml streptomycin and 50 U/ml penicillin, and cultured for additional 24 h. In a series of experiments, MG-132 (Merck) was added to the culture medium after 30 h of transfection at 1 μM for the remaining 18 h of the culture. The cells were harvested and stored as above.

Click chemistry

After 48 h of transfection with wild type mDGKε-Myc or its mutants, HEK293 cells were incubated with 50 μM 17ODYA (17-octadecynoic acid, Merck), added from stock solution in DMSO or 0.05% DMSO in DMEM containing 2% charcoal-stripped FBS and 30 mM HEPES for 4 h at 37°C, and processed essentially as described earlier (28). Briefly, harvested and pelleted cells were lysed in 300 μl of lysis buffer containing 0.5% SDS, 0.5% NP-40, 100 mM NaCl, 50 mM phosphate buffer, pH 7.4, 1 mM TCEP (Tris(2-carboxyethyl)phosphine hydrochloride), protease inhibitors (1 mM PMSF, 2 μg/ml aprotinin, 2 μg/ml leupeptin, and 0.7 μg/ml pepstatin), phosphatase inhibitor (1 mM Na_3VO_4), protein thioesterase inhibitors (10 μM palmostatin and 0.2 mM HDSF (1-hexadecanesulfonyl fluoride)) and 250 U/ml Benzonase Nuclease (Merck). After 30 min (4°C), the lysates were sheared by passing through a 25-G needle and clarified by centrifugation (4°C, 5 min, 14 500x*g*), and supernatants were diluted with five volumes of the lysis buffer without the detergents and TCEP, supplemented with 15 μl of Myc-Trap Agarose (with anti-Myc alpaca antibody) (Chromotek, cat. No. yta) and incubated for 3 h at 4°C with end-over-end rotation. Subsequently, samples were washed three times with ice-cold lysis buffer containing 0.05% NP-40 and once with lysis buffer without the detergent. Finally, the agarose beads were suspended in 50 μl of click reaction mixture containing 100 mM NaCl, 10 μM IRDye 800CW-azide (LI-COR, Lincoln), 1 mM TCEP, 100 μM Tris((1-benzyl-4-triazolyl)methyl)amine (TBTA), 1 mM $CuSO_4$, 50 mM phosphate buffer, pH 7.4, and protease inhibitors (cOmplete EDTA-free protease inhibitor cocktail (Roche), 1 mM PMSF, and 0.7 μg/ml pepstatin).

In a series of experiments, 5 mM methoxypolyethylene glycol azide (PEG-azide, Merck, catalog No. 689475) was used for the click reaction. After 1 h in the darkness with gentle rotation, samples were washed with lysis buffer containing 0.05% NP-40, and agarose beads were suspended in 40 µl of 2x SDS-sample buffer and heated for 10 min at 95°C. A subset of the 17ODYA-labeled samples were additionally incubated with 1 M hydroxylamine (HXA) for 30 min at 22°C and next diluted twice and incubated for 5 min at 100°C. Proteins were separated by 10% SDS-PAGE and analyzed in an Odyssey CLx Imager (LI-COR) and after that transferred onto nitrocellulose and subjected to immunoblotting.

Acyl-Biotin Exchange

The acyl-biotin exchange technique was applied to detect *S*-palmitoylation of DGKε essentially as described previously (35), with minor modifications. In brief, HEK293 cells were lysed in 500 µl of 150 mM NaCl, 5 mM EDTA, 1.7% Triton X-100, 4% SDS, cOmplete protease inhibitor cocktail, 2 mM PMSF, 250 U/ml Benzonase Nuclease, 50 mM Tris, pH 7.2, for 15 min 37°C with shaking, followed by sonication for 60 s (0.3 cycle; amplitude 33%; UP200S Hielscher sonifier). Lysate proteins were precipitated with chloroform:methanol:H_2O (1:4:3, v:v:v), dissolved in SDS buffer (4% SDS, 5 mM EDTA, 100 mM Hepes, pH 7.4) at 2 mg/ml and incubated with 5 mM TCEP and 20 mM methyl methanethiosulfonate (MMTS) for 15 min at 37°C and 20 min at 50°C, respectively, and precipitated three times as above. For biotinylation, the protein pellet was dissolved in 150 µl of the SDS buffer, diluted 20 times in a buffer containing 0.27 mM HPDP-biotin (ThermoFisher, Waltham, MA, USA), 0.27% Triton X-100, and 100 mM Hepes, pH 7.4. Each sample was halved, supplemented either with 1 M hydroxylamine (HXA+) or 50 mM Tris, pH 7.5 (HXA-) and incubated for 2 h at 20°C with agitation. Proteins were precipitated three times and solubilized as above, 20-µg aliquots were withdrawn as input samples, while 300 µg protein/sample was diluted 20 times in Triton buffer containing 150 mM NaCl, 0.2% Triton X-100, 20 mM Hepes, pH 7.4, 1 µg/ml leupeptin, aprotinin and pepstatin, 1 mM PMSF, 1 mM Na_3VO_4, 50 µM phenylarsine oxide, and supplemented with 50 µl of streptavidin-agarose (ThermoFisher). After 2 h of gentle agitation at 20°C, agarose beads were pelleted and washed 3 times in the Triton buffer without inhibitors. Finally, the beads

were suspended in 150 µl of elution buffer (150 mM NaCl, 0.2% SDS, 0.2% Triton X-100, 2% β-mercaptoethanol, 20 mM Hepes, pH 7.5) for 15 min (at 37°C with shaking) and subsequently in 100 µl of 1x SDS-sample buffer for 5 min (at 95°C with shaking). The two eluates were combined, and proteins precipitated with 4 volumes of cold acetone, dissolved in 30 µl of 2x SDS-sample buffer, denatured for 5 min at 95°C and subjected to 10% SDS-PAGE.

Acyl-PEG Exchange

To reveal the number of *S*-acylated cysteine residues in DGKε, the palmitic acid residue(s) of mDGKε-Myc were exchanged for polyethylene glycol (PEG) in the acyl-PEG exchange technique (APE, 36) which in principle resembles ABE. For this, HEK293 cells overexpressing mDGKε-Myc with selected zDHHC or GST for control were lysed, the lysates incubated with 5 mM TCEP and 20 mM MMTS with subsequent protein precipitation, as described above. The protein pellet was dissolved in 220 µl of the SDS buffer, protein concentration was adjusted to 2 mg/ml and then diluted 20 times with a buffer containing 0.27% Triton X-100 and 100 mM HEPES, pH 7.4, halved and supplemented or not with 1 M hydroxylamine (HXA+ or HXA-), and incubated for 2 h at 20°C with agitation. Protein was precipitated three times as above and finally dissolved in 100 µl of the SDS buffer. The samples were next supplemented with 100 µl of 4 mM methoxypolyethylene glycol maleimide (PEG-maleimide) (5000; Merck, catalog No. 63187) in the SDS buffer. After 2 h (20°C, with agitation), protein was precipitated 3 times and finally dissolved in 35 µl of the SDS buffer. Protein concentration was determined, samples were supplemented with 12 µl of 4x SDS-sample buffer, incubated for 5 min at 95°C, and subjected in equal amounts to 10% SDS-PAGE.

DGKε activity determination

The DGKε enzymatic activity assay was conducted according to previous studies (18). Briefly, 48 h after transfection, HEK293 cells were suspended in 300 µl of ice-cold homogenization buffer (0.25 M sucrose, 1 mM EDTA, 4 mM EGTA, 1 mM DTT, 20 mM Tris-HCl, pH 7.4, with 1 mM PMSF, 0.7 µg/ml pepstatin, 20 µg/ml aprotinin, and 20 µg/ml leupeptin) and sonicated. For micelle preparation, 1-NBD-stearoyl-2-

arachidonoyl-*sn*-glycerol (NBD-SAG, Cayman Chemical, cat. No. 10011300), SAG (Cayman Chemical, cat. No. 10008650) and 1,2-diacyl-*sn*-glycero-phosphoserine (PS, Merck, cat. No. P7769) dissolved in chloroform:methanol (2:1, v:v, with 30 µg/ml butylated hydroxytoluene as an antioxidant) were mixed at a 5:7 molar ratio of total SAG:PS. The total SAG contained 10% of NBD-SAG. The lipid mixture was dried and resuspended by vortexing (2 min, room temperature) in 4x reaction buffer containing 400 mM NaCl, 80 mM $MgCl_2$, 4 mM EGTA, 4 mM DTT, 300 mM octyl-β-glucoside (OG), 200 mM MOPS, pH 7.2, and supplemented with 2 mM ATP. Next, 15 µg of total protein in 40 µl of homogenization buffer was added to a reaction mixture containing 50 µl of the 4x reaction buffer with micelles and 110 µl of H_2O. The final concentrations of NBD-SAG/SAG in the reaction mixture was 1.45 or 4.46 mol% (0.75 mM or 2.5 mM) and of PS 2.03 or 6.25 mol% (1.05 mM or 3.5 mM). The DGKε activity assay was carried out for 10 min at 24°C with gentle agitation and stopped by the addition of 1 ml of methanol followed by 1 ml of chloroform and 0.7 ml of 1% perchloric acid. After phase separation, lower phase was washed two times with 2 ml of 1% perchloric acid and dried under a nitrogen stream. Lipids were dissolved in chloroform:methanol (2:1, v:v) and separated by TLC silica gel 60 (Merck) along with a standard, 0.5–100 pmol of 1-palmitoyl-2-NBDdodecanoyl-*sn*-glycero-3-phosphate (NBD-PDPA, Avanti, cat. No. 810174), with chloroform:methanol:acetic acid 80% (65:15:5, v:v:v) as mobile phase. NBD-lipids were visualized using G:Box (Syngene) and fluorescence intensity was assessed with ImageJ software using a standard curve drawn for NBD-PDPA and corrected by subtraction of background from samples transfected with empty vector. In parallel, cell homogenates were supplemented with 2% SDS, vortexed and incubated for 15 min, next supplemented with 1x SDS-sample buffer (final concentration), incubated again for 15 min, heated for 10 min at 95°C and subjected to SDS-PAGE alongside with 2 - 30 ng of GST-hDGKε (SignalChem, cat. No. D24–10G) and immunoblotting with sheep anti-DGKε antibody (R&D Systems).

SDS-PAGE and immunoblotting

Proteins were separated by SDS-PAGE and electrotransferred onto nitrocellulose, incubated with antibodies, and processed for detection by chemiluminescence as described previously (18, 28, 37). The

following antibodies were used: sheep anti-DGKε (R&D Systems, cat. No. AF7069), mouse anti-Myc (Invitrogen, cat. No. 46-0603 or Cell Signaling, cat. No. 2276), mouse anti-CD71 (transferrin receptor, Santa Cruse Biotechnology, cat. No. sc-32272), rabbit anti-Jak1 (Cell Signaling, cat. No. 3344), mouse anti-actin Ab-5 (BD Transduction Laboratories, cat. No. 612657), rabbit anti-flotillin-2 (Cell Signaling, cat. No. 3436), donkey anti-sheep IgG-HRP (Jackson ImmunoResearch Inc., cat. No. 713-035-003), mouse anti-HA IgG-HRP (Cell Signaling, cat. No. 2999), goat anti-mouse IgG-HRP (Jackson ImmunoResearch Inc., cat. No. 115-035-146) and goat anti-rabbit IgG-HRP (Merck, cat. No. 401315). Visualized bands were analyzed densitometrically using the ImageJ program. OD values were corrected by background subtraction which in the case of click chemistry included samples incubated with DMSO.

Data analysis

Student's *t*-test was used for the statistical analysis of data.

RESULTS

Cys 38/Cys40 is the major site of *S*-palmitoylation of mouse/human DGKε

In order to determine whether DGKε is palmitoylated, we cloned the *Dgke/DGKE* genes and modified them by adding the Myc tag at the C-terminus of the encoded proteins. We decided on such a location of the tag because amino acids 20-40/22-42 (mDGKε/hDGKε) from the N-terminus are predicted to form either a transmembrane or a U-shaped α-helix with Pro31/33 serving as a hinge (9) (Fig. 1A). Mouse DGKε-Myc was overexpressed in HEK293 cells and its palmitoylation was revealed by protein metabolic labeling with 17ODYA, a palmitic acid analogue subsequently tagged with a fluorescent dye by click-chemistry (Fig. 1B). Strong fluorescence of mDGKε-Myc was observed following its immunoprecipitate separation by SDS-PAGE for 17ODYA-labeled cells, which was virtually absent in a sample from mock-labeled cells (DMSO added instead of 17ODYA) (Fig. 1C). An equally minor mDGKε-Myc fluorescence was observed in another control sample in which the lysate of cells metabolically labeled with ODYA17 was treated with HXA cleaving the thioester bond (Supplemental Fig. S1A-C). The removal of 17ODYA from mDGKε-Myc by HXA indicated that mDGKε undergoes *S*-palmitoylation. In full agreement, an *S*-acylation of mDGKε-Myc was also found with the ABE technique which allows a selective capture of *S*-acylated proteins after substitution of their fatty acid residue(s) with biotin and enrichment on streptavidin beads (Fig. 1E, F). As expected, no mDGKε-Myc was detected in eluates from streptavidin beads incubated with samples not exposed to HXA which had precluded the biotinylation of originally *S*-acylated proteins (Fig. 1F).

To identify the site(s) of the *S*-palmitoylation of DGKε, we focused on its N-terminal region unique among all DGK isoenzymes. We reasoned that cysteine residue(s) located at the cytoplasmic end of the putative membrane-binding fragment are the most likely sites of DGKε *S*-palmitoylation; therefore, Cys26 or Cys38 of mDGKε-Myc were substituted with Ala (Fig. 1A). The Cys38Ala substitution nearly fully abolished the *S*-palmitoylation of mDGKε-Myc, as found with click chemistry and ABE. The trace *S*-acylation represented less than 7% of that found for wild type mDGKε (Fig. 1C, D and F, G). In contrast to Cys38Ala, the Cys26Ala mutation did not affect the *S*-palmitoylation of mDGKε-Myc (Fig. 1C, D and F, G). These data indicate that mDGKε is *S*-palmitoylated nearly exclusively at Cys38. Importantly, also

human DGKε was found with the ABE assay to be *S*-palmitoylated and Cys40 (corresponding to Cys38 in mDGKε) was identified as the site of this acylation, as evidenced by its abolishment by the Cys40Ala substitution (Fig. 1H).

Two other cysteine residues, Cys132 and Cys135, located in the C1B domain of mDGKε had earlier been suggested as sites of its *S*-palmitoylation by a global mouse forebrain *S*-palmitoylation site analysis (38). We therefore mutated each of them and found that the Cys132Ala mutation did not affect the *S*-palmitoylation of mDGKε while Cys135Ala led to its significant augmentation detected with both click chemistry and ABE (Fig. 1C, F, see also Fig. 2). We have recently found that Cys135 is an element of a zinc finger motif crucial for mDGKε activity and stability and its substitution with Ala leads to proteasomal degradation of the protein (18); indeed, the Cys135Ala mDGKε-Myc variant was present in small quantities which made its detection difficult (Fig. 1C, F, see also Fig. 2). In such conditions the reliability of the quantitation of the ratio of fluorescently- or biotin-labeled to total mDGKε-Myc protein amount is questionable; however, the hyperpalmitoylation of Cys135Ala mDGKε-Myc was confirmed robustly when the amount of the Cys135Ala mDGKε-Myc immunoprecipitate loaded on the gel was increased severalfold to equalize the amount of Cys135Ala mDGKε-Myc and wild type mDGKε-Myc (Supplemental Fig. S2A-E).

To confirm further that the mDGKε palmitoylation detected was indeed *S*-palmitoylation, the possibility of *O*-palmitoylation of mDGKε at serine residues Ser7 and Ser13 was investigated. These serine residues could be accessed by acyltransferases of the MBOAT family residing in the endoplasmic reticulum lumen (39, 40) and hypothetically capable of catalyzing *O*-palmitoylation of DGKε in a transmembrane conformation. Both Ser7 and Ser13 were substitutes with Ala in wild type or Cys135Ala mDGKε-Myc. These mutations did not affect palmitoylation of wild type mDGKε nor reduced the hyperpalmitoylation of Cys135Ala mDGKε, as found using click chemistry (Fig. 2A-C, Supplemental Fig. S2B-E) and ABE (Fig. 2F-H). These data argue against *O*-acylation of mDGKε, and indirectly confirm that we are dealing with *S*-palmitoylation, in agreement with the susceptibility of the mDGKε – palmitate linkage to HXA treatment.

Next, we substituted Lys354 with Ala, as this residue can be ubiquitinated (9), which could affect mDGKε *S*-palmitoylation, as has been observed for LRP6 (41). Again, no change of mDGKε *S*-palmitoylation was caused by the Lys354Ala substitution, including the hyperpalmitoylation of Cys135Ala / Lys354Ala mDGKε-Myc (Fig. 2B, C and G, H, Supplemental Fig. S2B, C). Notably, the hyperpalmitoylation was nearly abolished in the double Cys38Ala / Cys135Ala mutant, indicating that it resulted from the *S*-palmitoylation of a larger fraction of the kinase at the "regular" site (Cys38) rather than from acylation of cysteine residue(s) other than Cys38 (Fig. 2D, E and I, J).

Finally, we substituted Pro31 implied to affect the conformation of the N-terminus (4, 9) with Ala to assess its influence on DGKε *S*-palmitoylation. The Pro31Ala substitution decreased the steady-state mDGKε-Myc level, likely by affecting its stability (although to a lower extent than did the Cys135Ala substitution) and led to its hyperpalmitoylation; the latter was detected unequivocally with the click chemistry-based approach only (Fig. 2D, E and I, J, Supplemental Fig. S2D, E). When the proteasomal activity was inhibited with MG-132, all mDGKε forms were *S*-palmitoylated to a similar extent except for the barely modified Cys38Ala and Cys38Ala / Cys135Ala variants (Fig. 2D, E and I, J). Taken together, the data indicate that Cys38 is the predominant site of mDGKε *S*-palmitoylation, and the kinase mutated at Cys135 or Pro31 (likely misfolded and rapidly degraded by 26S proteasome) can be hyperpalmitoylated.

zDHHC7 and zDHHC17 can *S*-palmitoylate DGKε

Having detected the *S*-palmitoylation of mDGKε at Cys38, we aimed to determine which of the 23 mouse zDHHC enzymes could catalyze this reaction. To this end, we overproduced mDGKε-Myc together with each of these enzymes in HEK293 cells and after performing the ABE reaction the amount of mDGKε-Myc eluted from streptavidin beads was compared with that in controls with GST or empty vector in place of zDHHC. The amount of mDGKε-Myc recovered from the beads indicated the extent of its *S*-palmitoylation (Fig. 3A,B, Supplemental Fig. S3A, B). Note that in Fig. 3 the original nomenclature of the *S*-acyltransferases as DHHC is maintained (25, 34) which uses numbering of individual isoenzymes largely coincident with that preferred currently in the zDHHC nomenclature.

We found that the extent of *S*-palmitoylation of mDGKε-Myc was enhanced significantly in the presence of DHHC7 or DHHC17 (zDHHC7 and zDHHC17, respectively). The amount of mDGKε-Myc eluted from the beads in the presence of either *S*-acyltransferase increased by about 40% in comparison to the GST control (Fig. 3B, C). This increase was still as substantial when normalized to the amount of endogenous *S*-palmitoylated Jak1 (28) found in the eluates. The latter was not affected by the overproduction of zDHHC7 or zDHHC17 (Fig 3D, Supplemental Fig. S3C). At the same time also the amount of total mDGKε-Myc protein present in the input cell lysates (also when normalized to total Jak1) increased substantially, by 18% and 31%, respectively (Fig. 3B, E). As a consequence, the extent of mDGKε-Myc *S*-palmitoylation, i.e., the ratio of the amounts of *S*-palmitoylated mDGKε-Myc and total mDGKε-Myc protein, increased marginally in the case of zDHHC7 or remained virtually unchanged for zDHHC17 (Fig. 3F). Taken together, these results show that zDHHC7 and zDHHC17, located in the Golgi apparatus (24), can carry out *S*-palmitoylation of DGKε and thereby increase its abundance which suggests that the *S*-palmitoylation by these *S*-acyltransferases increases DGKε stability.

zDHHC7, 17 and 6/16 *S*-palmitoylate mDGKε at one cysteine residue

Next, we aimed to quantitate the fraction of the *S*-palmitoylated DGKε and verify the number of the *S*-acylation sites. For this, HEK293 cells co-transfected with mDGKε-Myc and selected zDHHCs (or GST for control) were subjected to the APE assay which relies on the substitution of cysteine-bound fatty acyls by the thiol-reactive PEG-maleimide leading to a stable PEGylation of the cysteines (36). The labeling of mDGKε-Myc with PEG slows its gel migration allowing simultaneous detection of the labeled (originally *S*-palmitoylated) and non-modified mDGKε-Myc (Fig. 4A).

We focused on zDHHC7 and zDHHC17 but, because the majority of DGKε is localized to the endoplasmic reticulum, we also included in those experiments zDHHC6 paired with zDHHC16. zDHHC6 is located exclusively in the endoplasmic reticulum and catalyzes *S*-palmitoylation of several local proteins under the control of zDHHC16 (42). To facilitate the subsequent quantitative analyses, in APE experiments

we used twice the amount of the mDGKε-Myc- and zDHHC-encoding plasmids for transfection relative to that used in the earlier ABE quantitative experiments shown in Fig. 3.

We found that in cells expressing mDGKε-Myc with the control GST about 20% of the kinase was modified with PEG reflecting its *S*-palmitoylation by endogenous zDHHC(s) (Fig. 4B-D). Importantly, Cys38Ala mDGKε-Myc was not PEGylated, indicating that Cys38 is the only site of mDGKε *S*-palmitoylation (Fig. 4B). These results were confirmed using a different method - click chemistry between 17ODYA and PEG-azide (Supplemental Fig. S4A-C). In the presence of zDHHC7 or zDHHC17 two phenomena were detected – the amount of *S*-palmitoylated mDGKε-Myc increased by as much as 5-fold above the GST control, which was accompanied by an increase in the abundance of non-palmitoylated mDGKε-Myc protein by about 65-80% (Fig. 4C, D). As a result, the fraction of PEGylated mDGKε-Myc increased to about 41-46% of the total protein. Bearing in mind the higher levels of ectopically-expressed mDGKε-Myc and zDHHCs in the present experiments, their results are in broad agreement with those of the earlier ones obtained using different methods of analysis (see Fig. 3). In the presence of zDHHC6/16, the increase in the abundance of *S*-palmitoylated mDGKε-Myc was also significant but lower - about 2.5-fold above the GST control. The amount of non-palmitoylated mDGKε-Myc also increased in these conditions (by about 40%), while the fraction of PEGylated mDGKε-Myc accounted for 32% of the total protein (Fig. 4C, D). As expected, when the Cys38Ala mDGKε-Myc was co-expressed with zDHHC7 instead of wild type kinase, no PEGylated (i.e., *S*-palmitoylated) form could be detected and the protein abundance remained unaffected (Fig. 4B). In all samples, the mass shift of PEGylated mDGKε-Myc corresponded to the binding of one PEG molecule per mDGKε-Myc molecule, as confirmed by an analysis of flotillin-1 PEGylation (not shown) which is known to be *S*-palmitoylated at a single cysteine (43). However, under conditions favoring strong mDGKε-Myc *S*-palmitoylation, as its co-expression with zDHH7 in Fig. 4C, an additional faint band appeared above the main one, which may indicate a second site of *S*-palmitoylation (Fig. 4C).

To ensure that the above observations are not unique to the mouse DGKε and are applicable to DGKε of other vertebrates as well, we assessed the *S*-palmitoylation of endogenous hDGKε in HEK293 cells (Fig.

4E, F). Up to 23% of hDGKε was PEGylated in cells not transfected with ectopic zDHHCs, resembling the percentage of modified mDGKε-Myc in corresponding samples. Again, only one site of hDGKε PEGylation was detected (Fig. 4F). The fraction of modified hDGKε did not change in the presence of overexpressed zDHHC7, 17 or 6/16 (Fig. 4F), which suggests that endogenous zDHHC(s) *S*-palmitoylated the kinase to the maximal level.

The Cys38Ala mutation moderately affects DGKε activity

The enzymatic activity of wild type, Cys38Ala and Pro31Ala forms of mDGKε-Myc was determined using NBD-SAG-containing mixed micelles and homogenates of HEK293 transfectants, as they were found previously optimal to investigating DGKε activity (18). The NBD-SAPA produced by DGKε was separated by TLC and related to the NBD-PDPA standard (Fig. 5A). In parallel, the content of the respective mDGKε-Myc protein in the homogenates was quantified by immunoblotting using GST-hDGKε as a standard (Fig. 5B). The specific activity of wild type mDGKε-Myc was about 11 pmol PA/min/ng DGKε at 1.45 mol% SAG and did not change when the latter was increased to 4.46 ml% (Fig. 5C). The Cys38Ala substitution increased the mDGKε-Myc activity by about 20% at 1.45 mol% SAG and by further 12% at 4.46 mol% SAG in comparison to the wild type kinase, yet the differences did not reach the statistical significance (Fig. 5C). In contrast, Pro31Ala substitution reduced the mDGKε-Myc activity significantly by 48% and 42% at 1.45 and 4.46 mol% SAG, respectively (Fig. 5C).

Discussion

The DGK family comprises ten isoenzymes catalyzing phosphorylation of DAG; their activity is likely fine-tuned by co/post-translational modifications. To date, however, the data on mouse/human DGKε modifications are limited to its ubiquitination at Lys354/357, a scarcity of information surprising in view of the obvious importance of DGKε as a participant in the PI cycle and a modulator of triglyceride metabolism in the endoplasmic reticulum (9, 44). Co/pos-translational modification of all other DGK are also poorly known, with the exception of phosphorylation (45). Our earlier study indicated that DGKε can undergo palmitoylation, as revealed by global palmitoylome analysis in Raw264 macrophage-like cells, when also an increase in the amount of palmitoylated mDGKε was detected in cells stimulated with LPS (28). In the present work, we reveal that m/hDGKε is *S*-palmitoylated at Cys38/40 and investigated various aspects of this modification in some detail.

Cys38/40 is located at the cytoplasmic site of a putative membrane-bound α-helix of m/hDGKε adopting possibly either a transmembrane topology or a U-shaped intramembrane one with Pro31/33 serving as hinge (9). It has been estimated that in about 95% of single-pass integral membrane proteins their palmitoylation site is located either at a juxtamembrane or an intramembrane cysteine (46), and DGKε fits the first model. Notably, the intramembrane Cys26/28 of m/hDGKε is not modified. Cys38 is by far the predominant site of DGKε *S*-palmitoylation but perhaps not the only one, as the Cys38Ala substitution eliminated about 93% of the modification detected with click and ABE, but not all of it. The sites(s) of this residual S-palmitoylation has not been determined nor is it known whether it even occurs in native DGKε. Our preliminary mass spectrometry analyses argue against such a possibility (not shown). There are as many as 28 cysteines in m/hDGKε. So far, no consensus sequence for protein *S*-acylation has been defined conclusively, but Cys72, 73, 75, 87, 88, 149 and 417 of mDGKε (and corresponding amino acids in hDGKε) are predicted by the SwissPalm database to undergo *S*-palmitoylation with high or medium confidence (https://swissplam.org, 24.01.2023). Notably, all those cysteines except for the latter one are localized to the cysteine-rich domains C1A (amino acids 58/60 - 106/108 in m/hDGKε) and C1B (amino acids 122/125 - 174/177) of the kinase. We have found recently that selected cysteine and histidine residues of the C1B

domain of mDGKε form a zinc-finger motif controlling the stability and activity of the kinase (18). Notably, Cys72/74 and 75/77 belong to an incomplete zinc finger motif lacking a His residue in the C1A domain, while Cys73/75, Cys87/89 and Cys 149/152 are not part of the respective motif in C1A and C1B domain (18, Fig. 5), potentially being available for *S*-acylation. A global proteomic analysis of *S*-acylated sites in proteins of the mouse forebrain indicated that Cys132 and Cys135 of the mDGKε C1B domain are modified (38), while our study excluded it. With all the above in mind, we tend to believe that some cysteine residue(s) of the C1A and C1B domains of DGKε can be prone to unspecific labeling at an excess of 17ODYA during metabolic labeling of cells (click technique) and being not reduced/blocked efficiently during the ABE procedure, allowing their subsequent biotinylation.

We identified zDHHC7, zDHHC17 and zDHHC6/16 as candidate mDGKε *S*-acyltransferases using the so-called "Fukata screen" (25, 34) followed by ABE and the APE assay. zDHHC7 and zDHHC17 were more effective than zDHHC6/16 in the model studies. The extent of DGKε *S*-palmitoylation by zDHHC7 and zDHHC17 increased profoundly when the amounts of plasmids encoding these proteins, used for transfection were doubled. These experimental data confirm the obvious otherwise supposition that the contribution of a particular isoenzyme to the *in vivo* modification of endogenous DGKε would be affected strongly by the possibility of their encounter. The identified zDHHCs differ substantially in their cellular localization, enzymatic activity and also preferences for the acyl-CoA species. zDHHC6 is found exclusively in the endoplasmic reticulum where also DGKε is unequivocally localized (47, 48). zDHHC6 catalyzes *S*-palmitoylation of crucial local proteins under the control of zDHHC16 which *S*-palmitoylates zDHHC6 potentially at three cysteine residues of its C-terminal region, with non-palmitoylated zDHHC6 being inactive. The two major *S*-palmitoylated forms of zDHHC6 are, respectively, highly active but short-lived and moderately active but more stable, pointing to a tight regulation of zDHHC6 functioning (42) which was also reflected by a very low level of zDHHC6 overexpression in our studies. On the other hand, zDHHC7 and zDHH17 locate in the *cis*-Golgi apparatus, as indicated by studies on human and mouse zDHHCs overexpressed in HEK293 and HeLa cells (24, 26). zDHHC7 has a high *S*-acyltransferase activity potentially towards multiple substrate proteins and prefers C14/C16 over C18 acyl-CoA. zDHHC17, with a

weaker enzymatic activity, utilizes preferentially the longer C16/C18 rather than C14 acyl-CoA species (49-51). The overexpression of zDHHCs and mDGKε could affect their cellular localization and 17ODYA used by us for metabolic labeling did not allow discriminating between C16 and C18 acyl chain as natural DGKε *S*-acylation substrates. All the above features are not sufficient to indicate which *S*-acyltransferase isoenzyme is responsible for DGKε acylation *in vivo*. It is of interest in this context that m/hDGKε carries the QP motif found in some zDHHC17 substrates allowing their recognition and binding by the ankyrin-repeat domain of the *S*-acyltransferase (51, 52), suggesting, though not proving (53) that DGKε could be a natural target of *S*-acylation by zDHHC17.

The detection of DGKε *S*-palmitoylation, which in HEK293 cells affects about one in four molecules of endogenous hDGKε, raises the question of its physiological significance. The most obvious effect of *S*-palmitoylation is the appearance of a hydrophobic anchor allowing or enhancing the binding of the modified protein to the membrane. Striking examples of such an effect are phosphoinositol 4-kinases IIα and IIβ, the former *S*-palmitoylated by zDHHC3 and zDHHC7 in the Golgi apparatus, which as a result of the *S*-palmitoylation acquire the properties of integral membrane proteins (54, 55). DGKε has a putative N-terminal transmembrane or re-entrant α-helix and the effects of the *S*-palmitoylation at the cysteine located in the cytoplasmic end of the α-helix can be analogous to those observed either for LRP6 or calnexin, both transmembrane proteins of the endoplasmic reticulum *S*-palmitoylated at juxtamembrane cysteines. *S*-palmitoylation of LRP6 (a protein involved in Wnt signaling) is likely to induce tilting of its transmembrane fragment thereby enabling an adjustment of its effective length to the thickness of the endoplasmic reticulum membrane (56). The consequences of S-palmitoylation for the conformation of calnexin, the endoplasmic reticulum chaperone which promotes the folding of glycoproteins, are more complex. The transmembrane fragment of calnexin is also predicted to be tilted in the membrane. Interestingly, the calnexin α-helix is additionally kinked due to the presence of a proline residue somewhat similar to Pro31/33 of m/hDGKε. *S*-palmitoylation of calnexin by zDHHC6 does not affect the proline-induced kink nor the α-helix tilt in the membrane. However, it is predicted to affect the orientation of its cytosolic fragment with respect to the α-helix axis and can favor the partitioning of calnexin to sheet-like perinuclear structures of the endoplasmic

reticulum. As a result, calnexin is properly positioned to capture its client proteins (23). Recent prediction of hDGKε structure indicates that the N-terminal fragment of the kinase is tilted in the membrane and its conformation determines the distance between its active site and the SAG-bearing membrane. It is proposed that the shortening of the distance, facilitating the kinase enzymatic activity, occurs as a result of bending of the transmembrane fragment at Pro33, and such conformational changes can be prevented by the interaction of the positively charged N-terminal amino acids of DGKε with PS in the membrane (4). It seems possible that *S*-palmitoylation of Cys38/40 cooperates with Pro31/33 in a similar manner. We found that the activity of Cys38Ala mDGKε-Myc mutant was moderately increased relative to that of wild type mDGKε-Myc which effect was likely underestimated as only about 20% of the wild type mDGKε-Myc was *S*-palmitoylated. These data are consistent with earlier finding that the whole N-terminal 50-amino-acid-long fragment of hDGKε comprising the transmembrane fragment and the following cluster of positively charged amino acids inhibited the kinase activity, as was determined using N-terminally truncated kinase mutant (4).

Our study also shows that the Pro31Ala mutation reduced DGKε activity markedly, in agreement with previous studies (3). In light of the model discussed, above this inhibition may result from hindering the conformational change of the DGKε N-terminus required for its activation. However, in our hands the Pro31Ala mutation also enhanced the protein degradation in a reproducible manner. We have recently found that certain mDGKε mutants, especially those in its C1B zinc finger, are inactive, likely misfolded, and degraded by 26S proteasome (18). The Pro31Ala substitution could have a global effect on DGKε folding (hence stability), thereby reducing its enzymatic activity. We base this assumption on the fact that the N-terminally truncated hDGKε had a higher activity but formed insoluble precipitates unless tagged at the N-terminus with His-SUMO (4), indicating an involvement of this DGKε fragment in maintaining proper protein conformation.

Our present study suggests that the *S*-palmitoylation of DGKε can affect its cellular transport and localization. A fraction of overexpressed DGKε was localized in the plasma membrane (3). Moreover, the plasma membrane rather than the endoplasmic reticulum has been indicated as the site of DGKε activity by

Balla's group who identified Nir2 as a phosphatidic acid transporter from the plasma membrane to the endoplasmic reticulum for further steps of the PI cycle (57, 58). Taking into account that DGKε can be *S*-palmitoylated by zDHHC7 and zHHC17, it is tempting to speculate that it undergoes this modification during its anterograde trafficking toward the plasma membrane. DGKε could resemble in this aspect the very well-studied hemagglutinin (HA) of the influenza A virus. HA is *S*-stearoylated at a cysteine located at a cytoplasmic end of its transmembrane fragment in the late endoplasmic reticulum or in *cis*-Golgi on its way to the plasma membrane for virion budding (59). Moreover, *S*-palmitoylation/acylation at the cytoplasmic end of transmembrane fragments has recently been identified as a signal guiding transmembrane proteins to the cisternal rims of the Golgi due to its impact on the shape of the transmembrane fragment (its conversion toward a cone-like one). Thanks to such sorting, acylated proteins are efficiently transported through the Golgi stacks to the plasma membrane (24) and similar trafficking of DGKε *S*-palmitoylated by zDHHC7 or zDHHC17 can be envisioned.

Finally, our data suggest a relationship between DGKε *S*-palmitoylation and stability. So far, both positive and negative effects of *S*-palmitoylation on protein stability have been reported (42, 60). In our hands, co-expression of zDHHC7 or zDHHC17 with wild type mDGKε led to an increase in the abundance of the kinase, while zDHHC6/16 were less effective in this matter. Up-regulated were both *S*-palmitoylated and non-palmitoylated forms of DGKε which can reflect the known DGKε tendency to dimerize (61). Reciprocally, a tendency for the reduction of the abundance of Cys38Ala mDGKε-Myc *vs.* wild type mDGKε-Myc was seen in some experiments (see Fig. 5). Additionally, the protective effect of *S*-palmitoylation on DGKε stability could explain the observed hyperpalmitoylation of the probably misfolded Cys135Ala and Pro31Ala kinase mutant forms. According to this scenario, upon inhibition of proteasomal activity by MG-132, the non-palmitoylated form would be enriched, which explains the disappearance of the hyperpalmitoylation. Thus, the DGKε mutants would resemble the LRP6 protein which, when misfolded, is retained in the endoplasmic reticulum due to ubiquitination and *S*-palmitoylation, which is conducive to restoring its native shape before the protein falls prey to the endoplasmic-reticulum-associated protein degradation (41).

Taken together, our data indicate that *S*-palmitoylation of DGKε at Cys38/40 can fine-tune its kinase activity and cellular level, and also suggest that a fraction of DGKε traffics through the Golgi apparatus toward the plasma membrane.

Data availability

The data that support findings of this study are available from the corresponding author on request.

Supplemental data

This article contains supplemental data.

Acknowledgements

We thank Prof. Masaki Fukata from the National Institute of Physiological Sciences in Okazaki, Japan for the library of vectors bearing DHHC1-23 *S*-acyltransferases. We thank Dr. Jan Fronk, formerly from the Faculty of Biology, University of Warsaw (retired) for helpful comments and critical discussion, and Dr. Anna Ciesielska and Dr. Orest V. Matveichuk from our Laboratory for valuable comments on the manuscript and preliminary study on the identification of zDHHC which can modify DGKε, respectively.

Funding sources

This work was supported by the National Science Centre, Poland (grant number 2018/29/B/NZ3/00407).

CRediT authorship contribution statement

Gabriela Traczyk: Conceptualization, Investigation, Formal analysis, Writing - Review & Editing. Aneta Hromada-Judycka: Investigation; Formal analysis; Writing - Review & Editing. Anna Świątkowska: Investigation, Formal analysis, Writing – Review & Editing. Julia Wiśniewska: Investigation, Writing - Review & Editing. Katarzyna Kwiatkowska: Conceptualization, Supervision, Project administration, Funding acquisition, Writing - Original draft preparation, Writing - Review & Editing.

Conflict of interest

The authors declare that they have no conflict of interest which could influence the work reported in this paper.

References

1. Sakane F., Imai, S., Kai, M., Yasuda, S., Kanoh, H. (2007) Diacylglycerol kinases: why so many of them? *Biochim Biophys Acta* 1771, 793-806. doi: 10.1016/j.bbalip.2007.04.006.

2. Franks, C.E., Campbell, S.T., Purow, B.W., Harris, T.E., Hsu, K.L. (2017) The ligand binding landscape of diacylglycerol kinases. *Cell Chem Biol* 24:870-880.e5. doi:10.1016/j.chembiol.2017.06.007.

3. Decaffmeyer, M,, Shulga, Y.V., Dicu, A.O., Thomas, A., Truant. R., Topham, M.K., Brasseur, R., Epand, R.M. (2008) Determination of the topology of the hydrophobic segment of mammalian diacylglycerol kinase ε in a cell membrane and its relationship to predictions from modeling. *J Mol Biol* 383:797-809. doi: 10.1016/j.jmb.2008.08.076.

4. Bozelli, J.C. Jr., Yune, J., Aulakh, S.S., Cao, Z., Fernandes, A., Seitova, A., Tong, Y., Schreier, S., Epand, R.M. (2022) Human diacylglycerol kinase ε N-terminal segment regulates the phosphatidylinositol cycle, controlling the rate but not the acyl chain composition of its lipid intermediates. ACS Chem Biol 17:2495-2506. doi: 10.1021/acschembio.2c00387.

5. Tang, W., Bunting, M., Zimmerman, G.A., McIntyre, T.M., Prescott, S.M.(1996) Molecular cloning of a novel human diacylglycerol kinase highly selective for arachidonate-containing substrates. *J Biol Chem* 271:10237–10241. https://doi. org/10.1074/jbc.271.17.10237.

6. Pettitt, T.R., Wakelam, M.J. (1999) Diacylglycerol kinase ε, but not ζ, selectively removes polyunsaturated diacylglycerol, inducing altered protein kinase C distribution in vivo. *J Biol Chem* 274:36181–36186. https://doi.org/10.1074/jbc.274.51.36181.

7. Lung, M., Shulga, Y.V., Ivanova, P.T., Myers, D.S., Milne, S.B., Brown, H.A., Topham, M. K., Epand, R.M. (2009) Diacylglycerol kinase ε is selective for both acyl chains of phosphatidic acid or diacylglycerol. *J Biol Chem* 284: 31062–31073. https://doi. org/10.1074/jbc.M109.050617

8. Ware, T.B., Franks, C.E., Granade, M.E., Zhang, M., Kim, K.B., Park, K.S., Gahlmann, A., Harris, T.E., Hsu, K.L. (2020) Reprogramming fatty acyl specificity of lipid kinases via C1 domain engineering. *Nat Chem Biol* 16:170–178. https://doi.org/10.1038/ s41589-019-0445-9.

9. Epand, R.M., So, V., Jennings, W., Khadka, B., Gupta, R.S., Lemaire, M. Diacylglycerol kinase-ε: properties and biological roles. (2016) *Front Cell Dev Biol* 4:112. https://doi.org/10.3389/fcell.2016.00112.

10. Rodriguez de Turco, E.B., Tang, W., Topham, M.K., Sakane, F., Marcheselli, V.L., Chen, C., Taketomi, A., Prescot, T.S.M., Bazan, N.G. (2001) Diacylglycerol kinase ε regulates seizure susceptibility and long-term potentiation through arachidonoyl-inositol lipid signaling. *Proc Natl Acad Sci U. S. A.* 98:4740–4745. https://doi. org/10.1073/pnas.081536298

11. Zhang, N., Li, B., Al-Ramahi, I., Cong, X., Held, J.M., Kim, E., Botas, J., Gibson, B.W., Ellerby, L.M. (2012) Inhibition of lipid signaling enzyme diacylglycerol kinase ε attenuates mutant huntingtin toxicity. *J Biol Chem* 287:21204–21213. https:// doi.org/10.1074/jbc.M111.321661.

12. Nakano, T., Seino, K., Wakabayashi, I., Stafforini, D.M., Topham, M.K., Goto.K. (2018) Deletion of diacylglycerol kinase ε confers susceptibility to obesity via reduced lipolytic activity in murine adipocytes. *FASEB J* 32:4121–4131. https://doi.org/ 10.1096/fj.201701050R.

13. Lemaire, M., Fr´emeaux-Bacchi, V., Schaefer, F., Choi, M., Tang, W.H., Le Quintrec, M., Fakhouri, F., Taque, S., Nobili, F., Martinez, F., Ji, W., Overton, J.D., Mane, S.M., Nürnberg, G., Altmüller, J., Thiele, H., Morin, D., Deschenes, G., Baudouin, V., Llanas, B., Collard, L., Majid, M.A., Simkova, E., Nürnberg, P., Rioux-Leclerc, N., Moeckel, G.W., Gubler, M.C., Hwa, J., Loirat, C., Lifton, R.P. (2013) Recessive mutations in DGKE cause atypical hemolytic-uremic syndrome. *Nat Genet* 45:531–536. https://doi.org/10.1038/ng.2590.

14. Liu, D., Ding, Q., Dai, D.F., Padhy, B., Nayak, M.K., Li, C., Purvis, M., Jin, H., Shu, C., Chauhan, A.K., Huang, C.L., Attanasio, M. (2021) Loss of diacylglycerol kinase ε causes thrombotic microangiopathy by impairing endothelial VEGFA signaling. *JCI Insight* 2021 6:146959. https://doi.org/10.1172/jci.insight.146959.

15. Shindo, M., Irie, K., Masuda, A., Ohigashi, H., Shirai, Y., Miyasaka, K., Saito, N. (2003) Synthesis and phorbol ester binding of the cysteine-rich domains of diacylglycerol kinase (DGK) isozymes. DGKγ and DGKβ are new targets of tumor-promoting phorbol esters. *J Biol Chem* 278:18448–18454. https://doi.org/10.1074/jbc. M300400200.

16. Shulga, Y.V., Topham, M.K., Epand, R.M. (2011) Study of arachidonoyl specificity in two enzymes of the PI cycle. *J Mol Biol* 409:101–112. https://doi.org/10.1016/j. jmb.2011.03.071.

17. Aulakh, S.S., Bozelli, J.C. Jr, Epand, R.M. (2022) Exploring the alpha fold predicted conformational properties of human diacylglycerol kinases. *J Phys Chem B* 126:7172-7183. doi: 10.1021/acs.jpcb.2c04533.

18. Traczyk, G., Świątkowska, A., Hromada-Judycka, A., Janikiewicz, J., Kwiatkowska, K. (2022) An intact zinc finger motif of the C1B domain is critical for stability and activity of diacylglycerol kinase-ε. *Int J Biochem Cell Biol* 152:106295. doi: 10.1016/j.biocel.2022.106295.

19. Bozelli, J.C., Jr, Jennings, W., Black, S., Hou, Y.H., Lameire, D., Chatha, P., Kimura, T., Berno, B., Khondker, A., Rheinst¨adter, M.C., Epand, R.M.(2018) Membrane curvature allosterically regulates the phosphatidylinositol cycle, controlling its rate and acyl-chain composition of its lipid intermediates. *J Biol Chem* 293:17780–17791. https://doi.org/10.1074/jbc.RA118.005293

20. Barylko, B., Mao, Y.S., Wlodarski, P., Jung, G., Binns, D.D., Sun, H.-Q., Yin, H.L., Albanesi, J.P. (2009) Palmitoylation controls the catalytic activity and subcellular distribution of phosphatidylinositol 4-kinase IIα. *J Biol Chem* 284:9994-10003. doi:10.1074/jbc.M900724200

21. Levental, I., Lingwood, D., Grzybek, M,. Coskun, U., Simons, K. (2010) Palmitoylation regulates raft affinity for the majority of integral raft proteins. *Proc Natl Acad Sci U. S. A.* 107:22050-22054. doi:10.1073/pnas.1016184107

22. Stepanek, O., Draber, P., Horejsi, V. (2014) Palmitoylated transmembrane adaptor proteins in leukocyte signaling. *Cell Signal* 26:895–902. doi:10.1016/j. cellsig.2014.01.007

23. Lakkaraju, A.K., Abrami, L., Lemmin, T, Blaskovic, S., Kunz, B., Kihara, A., Dal Peraro, M., van der Goot, F.G. (2012) Palmitoylated calnexin is a key component of the ribosome-translocon complex. *EMBO J* 31:1823-1835. doi:10.1038/emboj.2012.15

24. Ernst, A.M., Syed, S.A., Zaki, O., Bottanelli, F., Zheng, H., Hacke, M., Xi, Z., Rivera-Molina, F., Graham, M., Rebane, A.A., Björkholm, P., Baddeley, D., Toomre, D., Pincet, F., Rothman, J.E. (2018) *S*-Palmitoylation sorts membrane cargo for anterograde transport in the Golgi. *Dev Cell* 47:479-493.e7. doi: 10.1016/j.devcel.2018.10.024.

25. Fukata, M., Fukata, Y., Adesnik, H., Nicoll, R.A., Bredt, DS.. (2004) Identification of PSD-95 palmitoylating enzymes. *Neuron* 44(6):987-96. doi: 10.1016/j.neuron.2004.12.005.

26. Ohno, Y., Kihara, A., Sano, T., Igarashi, Y. (2006) Intracellular localization and tissue-specific distribution of human and yeast DHHC cysteine-rich domain-containing proteins. *Biochim Biophys Acta* 1761:474-483. doi:10.1016/j.bbalip.2006.03.010

27. Lemonidis, K., Werno, M.W., Greaves, J., Diez-Ardanuy, C., Sanchez-Perez, M.C., Salaun, C., Thomson, D.M., Chamberlain, L. (2015) The zDHHC family of *S*-acyltransferases. *Biochem Soc Trans* 43:217-221. doi:10.1042/BST20140270

28. Sobocińska, J., Roszczenko-Jasińska, P., Zaręba-Kozioł, M., Hromada-Judycka, A., Matveichuk, O.V., Traczyk, G., Łukasiuk, K., Kwiatkowska, K. (2018) Lipopolysaccharide upregulates palmitoylated enzymes of the phosphatidylinositol cycle: An insight from proteomic studies. Mol Cell Proteomics. 17:233-254. doi: 10.1074/mcp.RA117.000050.

29. Sobocińska, J., Roszczenko-Jasińska, P., Ciesielska, A., Kwiatkowska, K. (2018) Protein Palmitoylation and its role in bacterial and viral infections. *Front Immunol* J8:2003. doi: 10.3389/fimmu.2017.02003.

30. Hang, H.C., Geutjes, E.J., Grotenbreg, G., Pollington, A.M., Bijlmakers, M.J., Ploegh, H.L. (2007) Chemical probes for the rapid detection of fatty-acylated proteins in mammalian cells. *J Am Chem Soc* 129:2744–5. 10.1021/ja0685001.

31. Martin, B.R., Cravatt, B.F.(2009) Large-scale profiling of protein palmitoylation in mammalian cells. *Nat Methods* 6:135–8. 10.1038/nmeth.1293.

32. Drisdel, R.C., Alexander, J.K., Sayeed, A., Green, W.N. (2006) Assays of protein palmitoylation. *Methods* 40:127–34. 10.1016/j.ymeth.2006.04.015.

33. Roth, A.F., Wan, J., Bailey, A.O., Sun, B., Kuchar, J.A., Green, W.N., Phinney, B.S., Yates erd, J.R., Davis, N.G. (2006) Global analysis of protein palmitoylation in yeast. *Cell* 125:1003–13. 10.1016/j.cell.2006.03.042.

34. Fukata, Y., Iwanaga, T., Fukata, M. (2006) Systematic screening for palmitoyl transferase activity of the DHHC protein family in mammalian cells. *Methods* 40:177-82. doi: 10.1016/j.ymeth.2006.05.015.

35. Ziemlińska, E., Sobocińska, J., Świątkowska, A., Hromada-Judycka, A., Traczyk, G., Malinowska, A,, Świderska, B., Mietelska-Porowska, A., Ciesielska, A., Kwiatkowska, K. (20121) Palm oil-rich diet affects murine liver proteome and *S*-palmitoylome. *Int J Mol Sci* 22:13094. doi: 10.3390/ijms222313094.

36. Percher, A., Ramakrishnan, S., Thinon, E., Yuan, X., Yount, J.S., Hang, H.C. (2016) Mass-tag labeling reveals site-specific and endogenous levels of protein *S*-fatty acylation. *Proc Natl Acad Sci U. S .A.* 113:4302-7. doi: 10.1073/pnas.1602244113.

37. Prymas, K., Swiątkowska, A., Traczyk, G., Ziemli´nska, E., Dziewulska, A., Ciesielska, A., Kwiatkowska, K. (2020) Sphingomyelin synthase activity affects TRIF-dependent signaling of Toll-like receptor 4 in cells stimulated with lipopolysaccharide. *Biochim Biophys Acta Mol Cell Biol Lipids* 1865:158549. https://doi.org/10.1016/j. bbalip.2019.158549.

38. Collins, M.O., Woodley, K.T., Choudhary, J.S. (2017) Global, site-specific analysis of neuronal protein *S*-acylation. *Sci Rep* J7(1):4683. doi: 10.1038/s41598-017-04580-1.

39. Hofmann, K. (2000) A superfamily of membrane-bound *O*-acyltransferases with implications for Wnt signaling. *Trends Biochem Sci* 25:111-2. doi: 10.1016/s0968-0004(99)01539-x. PMID: 10694878.

40. Resh, M.D. (2016) Fatty acylation of proteins: The long and the short of it. *Prog Lipid Res* 63:120-31. doi: 10.1016/j.plipres.2016.05.002.

41. Perrody, E., Abrami, L., Feldman, M., Kunz, B., Urbé, S., van der Goot, F.G. (2016) Ubiquitin-dependent folding of the Wnt signaling coreceptor LRP6. *Elife* 2016 5:e19083. doi: 10.7554/eLife.19083. PMID: 27751231;

42. Abrami, L., Dallavilla, T., Sandoz, P.A., Demir, M., Kunz, B., Savoglidis, G,, Hatzimanikatis, V., van der Goot. F.G. (2017) Identification and dynamics of the human ZDHHC16-ZDHHC6 palmitoylation cascade. *Elife* 6:e27826. doi: 10.7554/eLife.27826.

43. Kwiatkowska, K., Matveichuk, O.V., Fronk, J., Ciesielska, A. (2020) Flotillins: At the intersection of protein *S*-palmitoylation and lipid-mediated signaling. *Int J Mol Sci* 21:2283. doi: 10.3390/ijms21072283.

44. Nakano, T., Goto, K. (2022) Diacylglycerol kinase ε in adipose tissues: A crosstalk between signal transduction and energy metabolism. *Front Physiol* 13:815085. doi:10.3389/fphys.2022.815085

45. Barbernitz, X., Raben. D.M.(2022) Phosphorylation of DGK. *Adv Biol Regul* 88:100941. doi: 10.1016/j.jbior.2022.100941.

46. Jiang, H., Zhang, X., Chen, X., Aramsangtienchai, P., Tong, Z., Lin, H. (2018) Protein lipidation: occurrence, mechanisms, biological functions, and enabling technologies. *Chem Rev* 118:919-988. doi: 10.1021/acs.chemrev.6b00750.

47. Kobayashi, N., Hozumi, Y., Ito, T., Hosoya, T., Kondo, H., Goto, K.(2007) Differential subcellular targeting and activity-dependent subcellular localization of diacylglycerol kinase isozymes in transfected cells. *Eur J Cell Biol* 86:433-44. doi: 10.1016/j.ejcb.2007.05.002.

48. Matsui, H., Hozumi, Y., Tanaka, T., Okada, M., Nakano, T,, Suzuki, Y., Iseki, K., Kakehata, S., Topham, M.K., Goto, K. (2014) Role of the N-terminal hydrophobic residues of DGKε in targeting the endoplasmic reticulum. *Biochim Biophys Acta* 1842S:1440-50. doi: 10.1016/j.bbalip.2014.07.007.

49. Lemonidis, K., Gorleku, O. A., Sanchez-Perez, M. C., Grefen, C. and Chamberlain, L. H. (2014) The Golgi S-acylation machinery comprises zDHHC enzymes with major differences in substrate affinity and *S*-acylation activity. *Mol Biol Cell* 25:3870-3883. doi:10.1091/mbc.e14-06-1169

50. Greaves, J., Munro, K.R., Davidson, S.C., Riviere, M., Wojno, J., Smith, T.K, Tomkinson, N.C., Chamberlain, L.H. (2017) Molecular basis of fatty acid selectivity in the zDHHC family of *S*-acyltransferases revealed by click chemistry. *Proc Natl Acad Sci U. S. A.* 114:E1365-E1374. doi: 10.1073/pnas.1612254114.

51. Lemonidis, K., Sanchez-Perez, M.C., Chamberlain, L.H. (2015) Identification of a novel sequence motif recognized by the ankyrin repeat domain of zDHHC17/13 *S*-acyltransferases. *J Biol Chem* 290:21939-50. doi: 10.1074/jbc.M115.657668.

52. Verardi, R., Kim, J.S., Ghirlando, R., Banerjee, A. (2017) Structural basis for substrate recognition by the ankyrin repeat domain of human DHHC17 palmitoyltransferase. *Structure* 25:1337-1347.e6. doi: 10.1016/j.str.2017.06.018.

53. Butler, L., Locatelli, C., Allagioti, D., Lousa, I., Lemonidis, K., Tomkinson, N.C.O., Salaun, C., Chamberlain, L.H. (2023) *S*-acylation of Sprouty and SPRED proteins by the *S*-acyltransferase zDHHC17 involves a novel mode of enzyme-substrate interaction. *J Biol Chem* 299:102754. doi: 10.1016/j.jbc.2022.

54. Jung, G., Wang, J., Wlodarski, P., Barylko, B., Binns, D.D., Shu, H., Yin, H.L., Albanesi, J.P. (2008) Molecular determinants of activation and membrane targeting of phosphoinositol 4-kinase IIβ. *Biochem J* 409:501-9. doi: 10.1042/BJ20070821

55. Lu, D., Sun, H.Q., Wang, H., Barylko, B., Fukata, Y., Fukata, M., Albanesi, J.P., Yin, H.L. (2012) Phosphatidylinositol 4-kinase IIα is palmitoylated by Golgi-localized palmitoyltransferases in cholesterol-dependent manner. *J Biol Chem* 287:21856-65. doi: 10.1074/jbc.M112.348094.

56. Abrami, L., Kunz, B., Iacovache, I, van der Goot, F.G. (2008) Palmitoylation and ubiquitination regulate exit of the Wnt signaling protein LRP6 from the endoplasmic reticulum. *Proc Natl Acad Sci U. S. A.* 105:5384–5389. doi: 10.1073/pnas.0710389105.

57. Kim, Y.J., Guzman-Hernandez, M.L., Wisniewski, E., Balla, T. (2015) Phosphatidylinositol-phosphatidic acid exchange by Nir2 at ER-PM contact sites maintains phosphoinositide signaling competence. *Dev Cell* 33:549-61. doi: 10.1016/j.devcel.2015.04.028.

58. Kim, Y.J., Guzman-Hernandez, M.L., Wisniewski, E., Echeverria, N., Balla, T. (2016) Phosphatidylinositol and phosphatidic acid transport between the ER and plasma membrane during PLC activation requires the Nir2 protein. *Biochem Soc Trans* 44:197-201. doi: 10.1042/BST20150187.

59. Veit, M., Serebryakova, M.V., Kordyukova, L.V. (2013) Palmitoylation of influenza virus proteins. *Biochem Soc Trans* 41:50-5. doi: 10.1042/BST20120210.

60. Locatelli C, Lemonidis K, Salaun C, Tomkinson NCO, Chamberlain LH. Identification of key features required for efficient *S*-acylation and plasma membrane targeting of sprouty-2. (2020) *J Cell Sci* 133doi:jcs249664. doi: 10.1242/jcs.249664.

61. Dicu, A.O., Topham, M.K., Ottaway, L., Epand, R.M. (2007) Role of the hydrophobic segment of diacylglycerol kinase ε. *Biochemistry* 46:6109–6117. https://doi.org/ 10.1021/bi6024726.

Figure legends

Figure 1. DGKε is *S*-palmitoylated at the cysteine located at the cytosolic end of its N-terminal transmembrane fragment. (A) The amino acid sequence of the N-terminal fragment of human and mouse DGKε. Amino acids mutated in this study are indicated by red font. The predicted transmembrane fragment is indicated by the solid line**.** The complete mDGKε/hDGKε consists of 564/567 amino acids. **(B)** Scheme of the click chemistry procedure. **(C, D, F, G, H)** HEK293 cells were transfected with plasmid encoding wild type mDGKε-Myc (**C, D, F, G**) or hDGKε-Myc (**H**) or their indicated mutant forms. **(C, D)** After 48 h, cells were subjected to metabolic labeling with 50 μM 17ODYA or exposed to 0.05% DMSO carrier as control (-17ODYA) for 4 h and lysed. mDGKε-Myc was immunoprecipitated with anti-Myc alpaca antibody and subjected to click chemistry reaction with IRDye 800CW-azide. (**C, upper panel**) In-gel fluorescence showing mDGKε-Myc labeling with 17ODYA followed by IRDye-azide. (**C, lower panels**) Efficiency of immunoprecipitation determined by immunoblotting with mouse anti-Myc antibody. The content of mDGKε-Myc and actin in input lysates is shown on the right**.** Arrowhead indicates a band recognized unspecifically by the anti-Myc antibody. **(D)** The extent of mDGKε-Myc palmitoylation. mDGKε-Myc fluorescence was determined by densitometry and normalized against the content of respective Myc-tagged kinase variant in immunoprecipitates. **(E)** Scheme of the ABE procedure. **(F, G, H)** After 48 h of transfection, cells were lysed and proteins were subjected to the ABE procedure involving treatment with hydroxylamine (HXA+) or not (HXA-), biotinylation, and capture of originally *S*-palmitoylated proteins on streptavidin-agarose beads. **(F, H, upper panels)** *S*-palmitoylated mDGKε-Myc **(F)** and hDGKε-Myc **(H)** eluted from the streptavidin-agarose beads revealed with mouse anti-Myc antibody. (**F, H, lower panels)** Transferrin receptor (Tfr), an *S*-acylated protein, eluted from the beads. The content of total mDGKε-Myc, hDGKε-Myc and TfR in input lysates is shown on the right. **(G)** The extent of mDGKε-Myc *S*-palmitoylation. The content of mDGKε-Myc in eluates and in input lysates was determined by densitometry, normalized against TfR and the ratio of *S*-palmitoylated mDGKε-Myc (eluates) to total mDGKε-Myc (lysates) is shown. ev, empty vector. Molecular weight markers are shown

on the right. Data shown are mean ± SD from four experiments. *, ***, Significantly different at $p = 0.05$ and $p < 0.001$, respectively, from cells expressing wild type DGKε.

Figure 2. Cys38 is the predominant site of mDGKε *S*-palmitoylation. HEK293 cells were transfected with plasmid encoding wild type mDGKε-Myc or its indicated mutant forms and subjected to click chemistry or ABE. **(A)** Scheme of the click chemistry procedure. **(B-E)** After 48 h, cells were subjected to metabolic labeling with 50 μM 17ODYA or exposed to 0.05% DMSO carrier as control (-17ODYA) for 4 h and lysed. **(D, E)** When indicated, prior to lysis cells were treated with the proteasomal inhibitor MG-132 (1 μM, 18 h). mDGKε-Myc was immunoprecipitated with anti-Myc alpaca antibody and subjected to click chemistry reaction with IRDye 800CW-azide. **(B, D, upper panels)** In-gel fluorescence showing mDGKε-Myc labeling with 17ODYA followed by IRDye-azide. **(B, D, lower panels)** Efficiency of immunoprecipitation determined by immunoblotting with mouse anti-Myc antibody. The content of mDGKε-Myc and actin in input lysates is shown on the right**.** Arrowhead indicates a band recognized unspecifically by the anti-Myc antibody. **(C, E)** The extent of mDGKε-Myc palmitoylation. mDGKε-Myc fluorescence was determined by densitometry and normalized against the content of respective Myc-tagged kinase variants in immunoprecipitates. **(F)** Scheme of the ABE procedure. **(G-J)** After 48 h of transfection, cells were lysed and proteins subjected to the ABE procedure involving treatment with hydroxylamine (HXA+) or not (HXA-), biotinylation, and capture of originally *S*-palmitoylated proteins on streptavidin-agarose beads. **(I, J)** When indicated, prior to lysis cells were treated with MG-132 (1 μM, 18 h)**. (G, I, upper panels)** *S*-palmitoylated mDGKε-Myc eluted from streptavidin-agarose beads revealed with mouse anti-Myc antibody. **(G, I, lower panels)** Transferrin receptor (Tfr), an *S*-acylated protein, eluted from the beads. The content of total mDGKε-Myc and TfR in input lysates is shown on the right. In **(I)** MG-132-treated samples were loaded at half the amount of protein from non-treated samples to avoid overloading. **(H, J)** The extent of mDGKε-Myc *S*-palmitoylation. The content of mDGKε-Myc in eluates and in input lysates was determined by densitometry, normalized against TfR and the ratio of *S*-palmitoylated mDGKε-Myc (eluates) to total mDGKε-Myc (lysates) is shown. ev, empty vector. Molecular weight markers are

shown on the right. Data shown are mean ± SD from four (C, J) or three (E, H) experiments. * and $^{\$}$; **, $^{\#\#}$, and $^{\$\$}$; $^{\#\#\#}$, significantly different at $p < 0.05$; $p < 0.01$; and $p < 0.001$, respectively, from cells expressing wild type mDGKε-Myc (*, **), wild type mDGKε-Myc in MG-132-treated cells ($^{\#\#}$, $^{\#\#\#}$). ($^{\$, \$\$}$) indicate the difference significance between MG-132-treated and untreated cells.

Figure 3. DGKε can be *S*-palmitoylated by zDHHC7 and zDHHC17. HEK293 cells were co-transfected with plasmids encoding wild type mDGKε-Myc and one of the mouse *S*-acyltransferases DHHC1 - 23 tagged with HA, or with GST-HA or empty vector (ev) in controls. After 24 h, cells were lysed and proteins were subjected to the ABE procedure involving treatment with hydroxylamine (HXA+) or not (HXA-), biotinylation, and capture of originally *S*-palmitoylated proteins on streptavidin-agarose beads**. (A)** Scheme of the ABE procedure. **(B)** *S*-palmitoylated mDGKε-Myc (upper panels) and Jak1 (lower panels) eluted from the streptavidin-agarose beads revealed with sheep anti-DGKε and rabbit anti-Jak1 antibody, respectively. The content of mDGKε- and Jak1 in input lysates is shown on the right. NT, cells not transfected. A faint band seen in some panel below mDGKε-Myc represents endogenous hDGKε. Eluates obtained from cells co-expressing mDGKε-Myc and DHHC7 or DHHC17 are boxed in yellow. **(C, D)** The content of *S*-palmitoylated mDGKε-Myc in eluates was determined by densitometry **(C)** and normalized against *S*-palmitoylated Jak1 for cells co-expressing mDGKε-Myc and DHHC7 or DHHC17 **(D)**. **(E)** The content of total mDGKε-Myc in input lysates normalized against total Jak1. **(F)** The extent of mDGKε-Myc *S*-palmitoylation in cells co-expressing mDGKε-Myc and zDHHC7 or zDHHC17. The content of mDGKε-Myc in eluates and in input lysates was normalized against Jak1 and the ratio of *S*-palmitoylated mDGKε-Myc (eluates) to total mDGKε-Myc (lysates) is shown. Molecular weight markers are shown on the right. Data shown are mean ± SD from three - five experiments (C, E), in (E) run in duplicates (HXA+ and HXA-), and from five and four experiments with DHHC7 and DHHC17, respectively (D, F). * and **, significantly different at $p < 0.05$ and $p < 0.01$, respectively, from cells co-expressing mDGK-Myc and GST-HA. In (C, E) the values for GST-expressing cells are averages for all samples tested while the significance of differences was evaluated by comparing values for cells expressing given DHHC with those from GST-

expressing cells analyzed on the same gels. DHHC are numbered after Fukata et al. (25, 34), DHHC10, 11, 13, 22 and 23 correspond to zDHHC11, 23, 24, 13 and 25, respectively.

Fig. 4. zDHHC7, 17 and 6/16 *S*-palmitoylate DGKε at one cysteine residue. (A-D) HEK293 cells were transfected with plasmids encoding wild type mDGKε-Myc or Cys38Ala mDGKε-Myc together with indicated zDHHC-HA or GST-HA in controls. After 24 h, cells were lysed and proteins were subjected to the APE procedure involving treatment with hydroxylamine (HXA+) or not (HXA-) and incubation with PEG-maleimide. **(A)** Scheme of the APE procedure. **(B, C)** mDGKε-Myc (upper panels) and actin (lower panels) in cell lysates revealed with mouse anti-Myc and mouse anti-actin antibody, respectively. NT, cells not transfected. Arrowhead indicates a band recognized unspecifically by the anti-Myc antibody. **(D)** The extent of DGKε *S*-palmitoylation. The content of PEGylated (originally *S*-palmitoylated) and non-palmitoylated mDGKε-Myc was determined by densitometry and normalized against actin. Data are mean ± SD from four experiments. *, ***, significantly different at $p < 0.05$ and $p < 0.001$, respectively, from *S*-palmitoylated form in cells co-expressing mDGKε-Myc and GST-HA; ##, significantly different at $p < 0.01$ from non-palmitoylated form in cells co-expressing mDGKε-Myc and GST-HA. **(E, F)** HEK293 cells were transfected with plasmid encoding indicated zDHHC-HA or GST-HA in controls. After 24 h, cells were lysed and proteins were subjected to the APE procedure. **(E)** Scheme of the APE procedure. **(F)** Endogenous hDGKε (upper panel) and actin (lower panel) in cell lysates revealed with sheep anti-DGKε and mouse anti-actin antibody, respectively. Numbers below blots indicate amount of palmitoylated and non-palmitoylated endogenous hDGKε determined as in (D). Molecular weight markers are shown on the right.

Fig. 5. The Cys38Ala substitution moderately affects DGKε activity. HEK293 cells were transfected with indicated mDGKε-Myc variants or with empty vector (ev) for 48 h, homogenized by sonication, and DGKε activity was determined in the homogenates using a fluorescence assay with mixed micelles of 1.45:2.03 mol% or 4.46:6.25 mol% NBD-SAG/SAG:PS. **(A)** Representative TLC separation revealing

`NBD-SAPA produced in homogenates of mDGKε-Myc-expressing and control cells. Reactions were carried out using 15 μg of total protein per sample, SAG was used at indicated mol%. Lipids from 1/50 of the reaction mixture were separated by TLC. NBD-PDPA is used as a standard, it migrates more slowly on TLC than NBD-SAPA. **(B)** Content of indicated overexpressed mDGKε-Myc variants (upper panel) and actin (lower panel) in cell homogenates revealed by immunoblotting with sheep anti-DGKε and mouse anti-actin antibody, respectively. GST-hDGKε is used as a standard. Three micrograms of total protein was applied per lane. **(C)** Specific activity of indicated mDGKε-Myc variants calculated after subtraction of the activity of endogenous DGKs determined in homogenate from control cells (ev). Molecular weight standards are shown on the right. Data are mean ± SD from eight (1.45 mol% SAG) or four (4.46 mol% SAG) experiments. * and **, significantly different at $p < 0.05$ and $p < 0.01$, respectively, from samples of wild type mDGKε-Myc analyzed at corresponding mol% SAG.

Figure 1

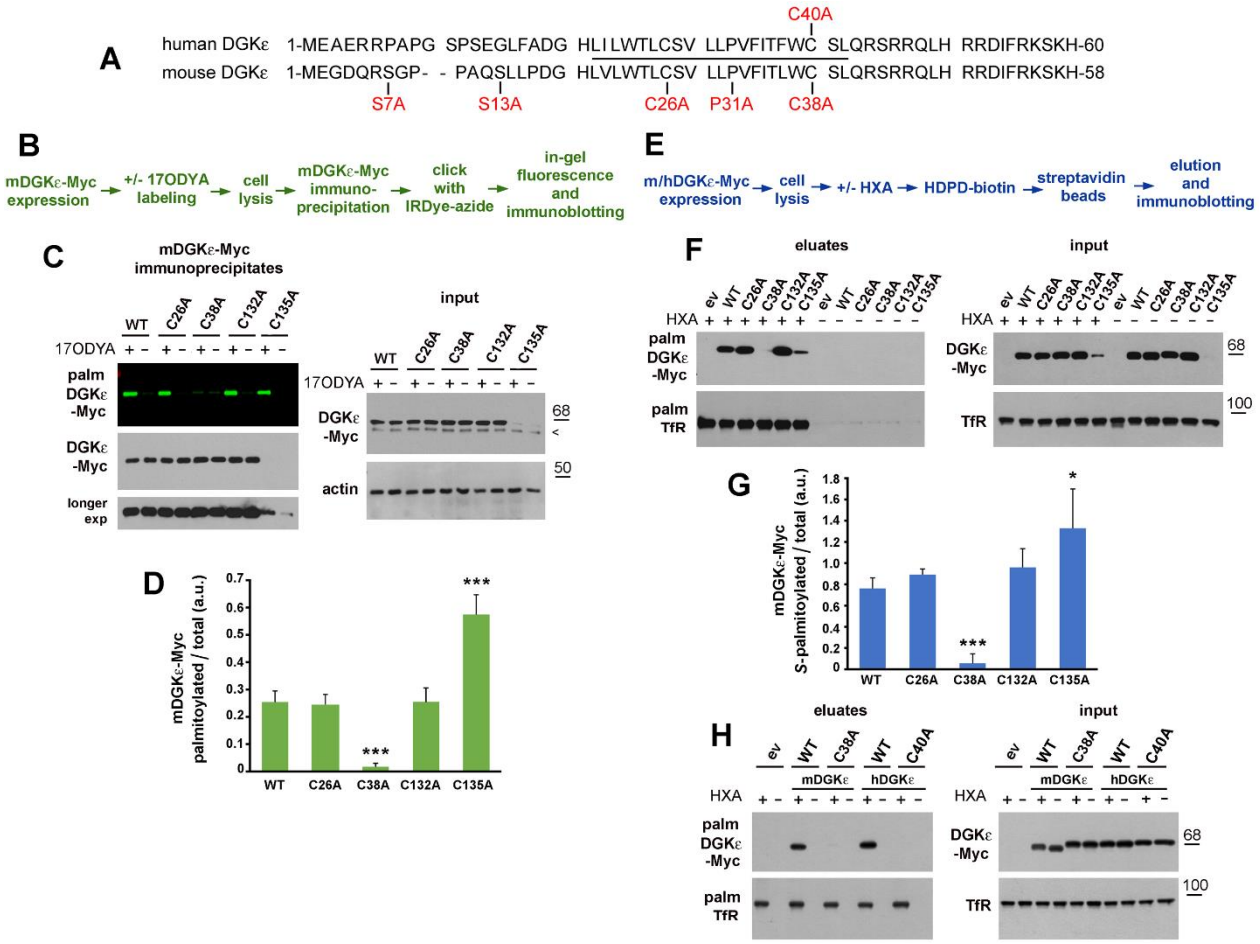
A
C40A
human DGKε 1-MEAERRPAPG SPSEGLFADG HLILWTLCSV LLPVFITFWC SLQRSRRQLH RRDIFRKSKH-60
mouse DGKε 1-MEGDQRSGP- - PAQSLLPDG HLVLWTLCSV LLPVFITLWC SLQRSRRQLH RRDIFRKSKH-58
S7A
S13A
C26A
P31A
C38A
B
mDGKε-Myc expression
+/- 17ODYA labeling
cell lysis
mDGKε-Myc immuno-precipitation
click with IRDye-azide
in-gel fluorescence and immunoblotting
E
m/hDGKε-Myc expression
cell lysis
+/- HXA
HDPD-biotin
streptavidin beads
elution and immunoblotting
C
mDGKε-Myc immunoprecipitates
input
WT
C26A
C38A
C132A
C135A
17ODYA
palm DGKε -Myc
DGKε -Myc
longer exp
actin
68
50
D
mDGKε-Myc palmitoylated / total (a.u.)
***
F
eluates
input
ev
HXA
palm DGKε -Myc
palm TfR
TfR
100
G
S-palmitoylated / total (a.u.)
*
H
mDGKε
hDGKε
C40A

Figure 2

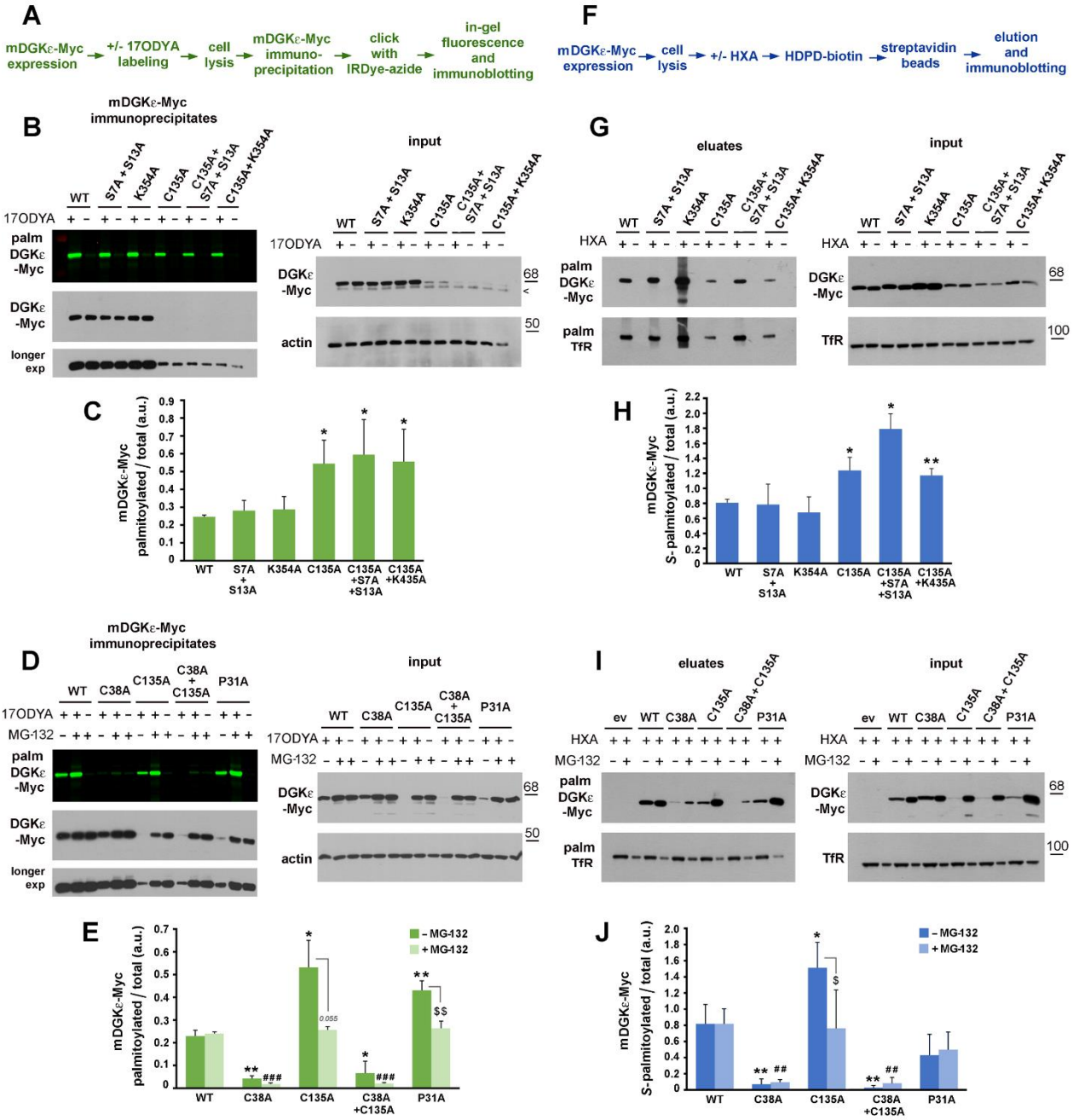
A
mDGKε-Myc expression
+/- 17ODYA labeling
cell lysis
mDGKε-Myc immuno-precipitation
click with IRDye-azide
in-gel fluorescence and immunoblotting
F
mDGKε-Myc expression
cell lysis
+/- HXA
HDPD-biotin
streptavidin beads
elution and immunoblotting
B
mDGKε-Myc immunoprecipitates
input
WT
S7A + S13A
K354A
C135A
C135A + S7A + S13A
C135A+K354A
17ODYA
palm DGKε -Myc
DGKε -Myc
longer exp
actin
68
50
G
eluates
input
HXA
palm TfR
TfR
100
C
mDGKε-Myc palmitoylated / total (a.u.)
WT
S7A + S13A
K354A
C135A
C135A +S7A +S13A
C135A +K435A
H
S-palmitoylated / total (a.u.)
D
C38A
C135A
C38A + C135A
P31A
MG-132
E
– MG-132
+ MG-132
0.055
I
ev
J

Figure 3

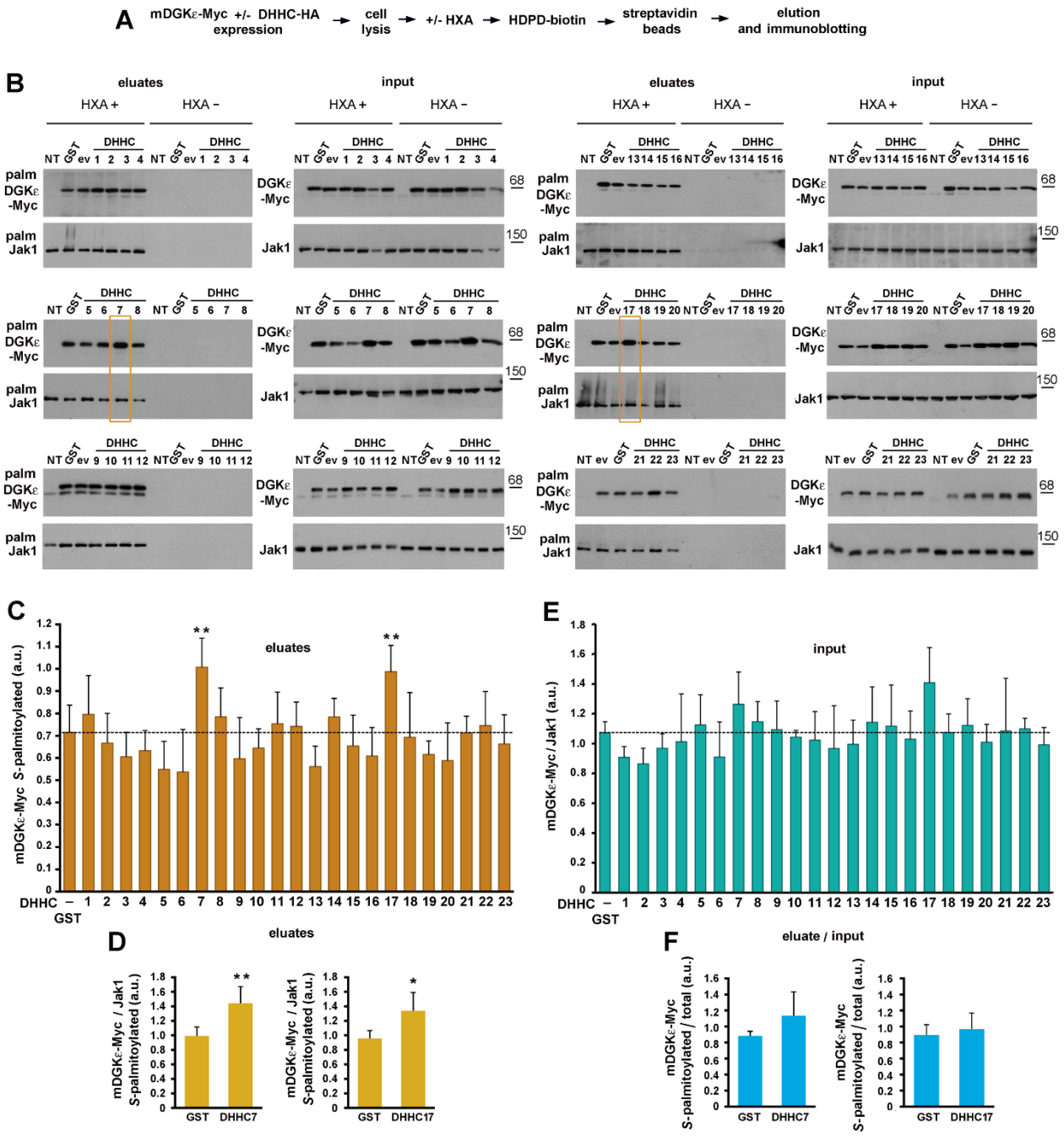
A
mDGKε-Myc +/- DHHC-HA expression
cell lysis
+/- HXA
HDPD-biotin
streptavidin beads
elution and immunoblotting
B
eluates
input
HXA +
HXA −
palm DGKε -Myc
palm Jak1
DGKε -Myc
Jak1
68
150
C
eluates
mDGKε-Myc S-palmitoylated (a.u.)
DHHC
GST
D
eluates
mDGKε-Myc / Jak1 S-palmitoylated (a.u.)
GST
DHHC7
DHHC17
E
input
mDGKε-Myc / Jak1 (a.u.)
F
eluate / input
mDGKε-Myc S-palmitoylated / total (a.u.)

Figure 4

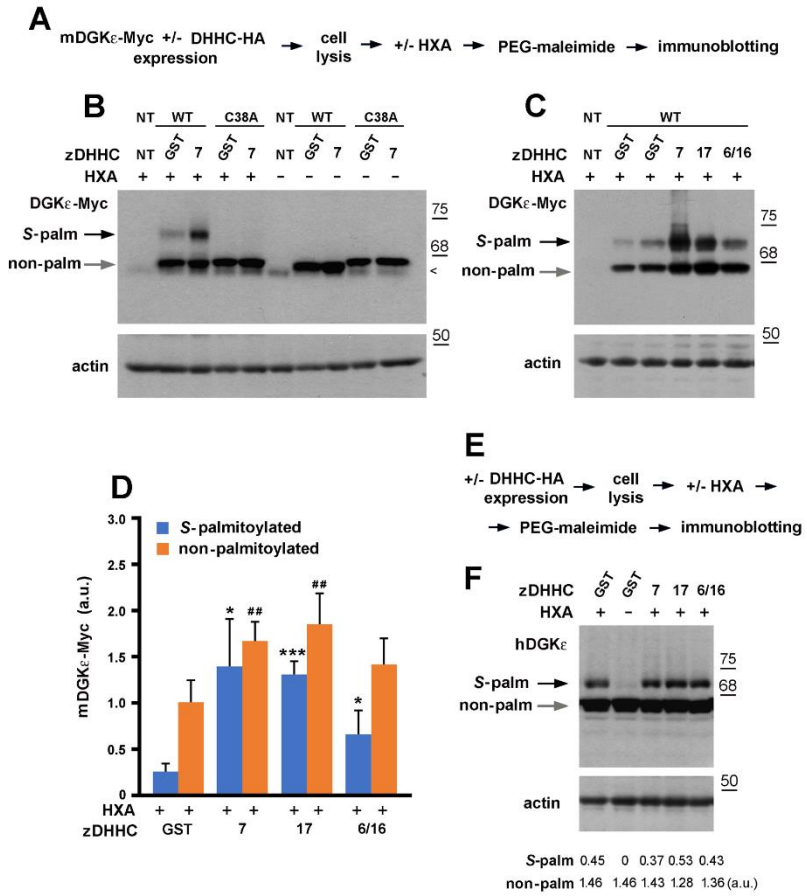
A
mDGKε-Myc +/- DHHC-HA expression
cell lysis
+/- HXA
PEG-maleimide
immunoblotting
B
NT WT C38A NT WT C38A
zDHHC NT GST 7 GST 7 NT GST 7 GST 7
HXA + + + + + - - - - -
DGKε-Myc
S-palm
non-palm
actin
75
68
50
C
NT WT
zDHHC NT GST GST 7 17 6/16
HXA + + + + + +
DGKε-Myc
S-palm
non-palm
actin
75
68
50
D
S-palmitoylated
non-palmitoylated
mDGKε-Myc (a.u.)
3.0
2.5
2.0
1.5
1.0
0.5
0
*
##
***
##
*
HXA + + + + + + + +
zDHHC GST 7 17 6/16
E
+/- DHHC-HA expression
cell lysis
+/- HXA
PEG-maleimide
immunoblotting
F
zDHHC GST GST 7 17 6/16
HXA + - + + +
hDGKε
S-palm
non-palm
actin
75
68
50
S-palm 0.45 0 0.37 0.53 0.43
non-palm 1.46 1.46 1.43 1.28 1.36 (a.u.)

Figure 5

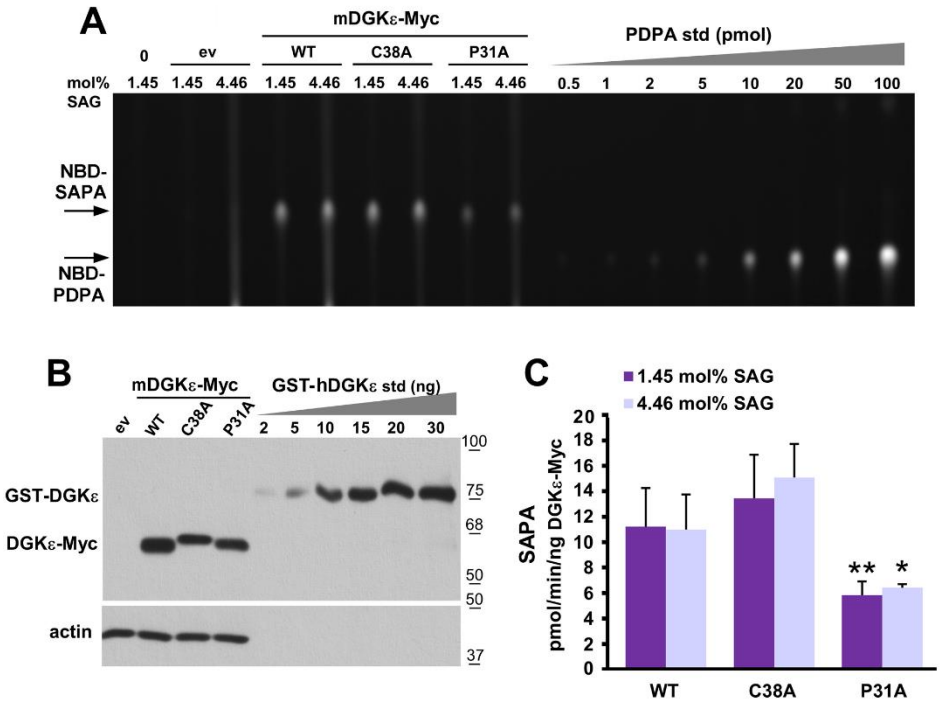
A
mDGKε-Myc
0
ev
WT
C38A
P31A
PDPA std (pmol)
mol% SAG
1.45 1.45 4.46 1.45 4.46 1.45 4.46 1.45 4.46
0.5 1 2 5 10 20 50 100
NBD-SAPA
NBD-PDPA
B
mDGKε-Myc
GST-hDGKε std (ng)
ev WT C38A P31A
2 5 10 15 20 30
GST-DGKε
DGKε-Myc
actin
100
75
68
50
50
37
C
1.45 mol% SAG
4.46 mol% SAG
SAPA
pmol/min/ng DGKε-Myc
20 18 16 14 12 10 8 6 4 2 0
**
*
WT
C38A
P31A

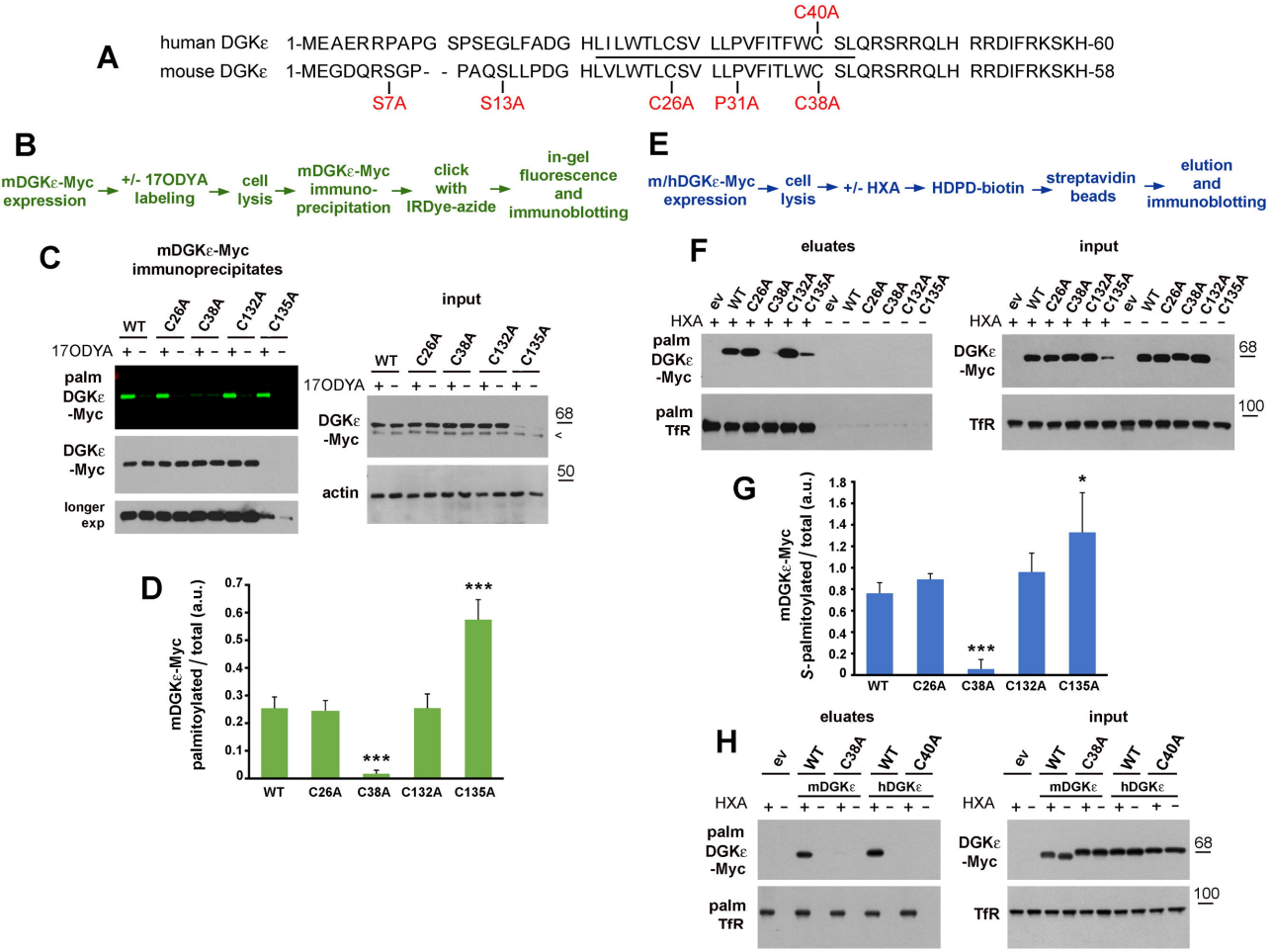
A
C40A
human DGKε 1-MEAERRPAPG SPSEGLFADG HLILWTLCSV LLPVFITFWC SLQRSRRQLH RRDIFRKSKH-60
mouse DGKε 1-MEGDQRSGP- - PAQSLLPDG HLVLWTLCSV LLPVFITLWC SLQRSRRQLH RRDIFRKSKH-58
S7A
S13A
C26A
P31A
C38A
B
mDGKε-Myc expression
+/- 17ODYA labeling
cell lysis
mDGKε-Myc immuno-precipitation
click with IRDye-azide
in-gel fluorescence and immunoblotting
E
m/hDGKε-Myc expression
cell lysis
+/- HXA
HDPD-biotin
streptavidin beads
elution and immunoblotting
C
mDGKε-Myc immunoprecipitates
WT
C26A
C38A
C132A
C135A
17ODYA
palm DGKε -Myc
DGKε -Myc
longer exp
input
actin
68
50
D
mDGKε-Myc palmitoylated / total (a.u.)
***
WT
C26A
C38A
C132A
C135A
F
eluates
input
ev
HXA
palm DGKε -Myc
palm TfR
TfR
68
100
G
mDGKε-Myc S-palmitoylated / total (a.u.)
*
H
mDGKε
hDGKε
C40A

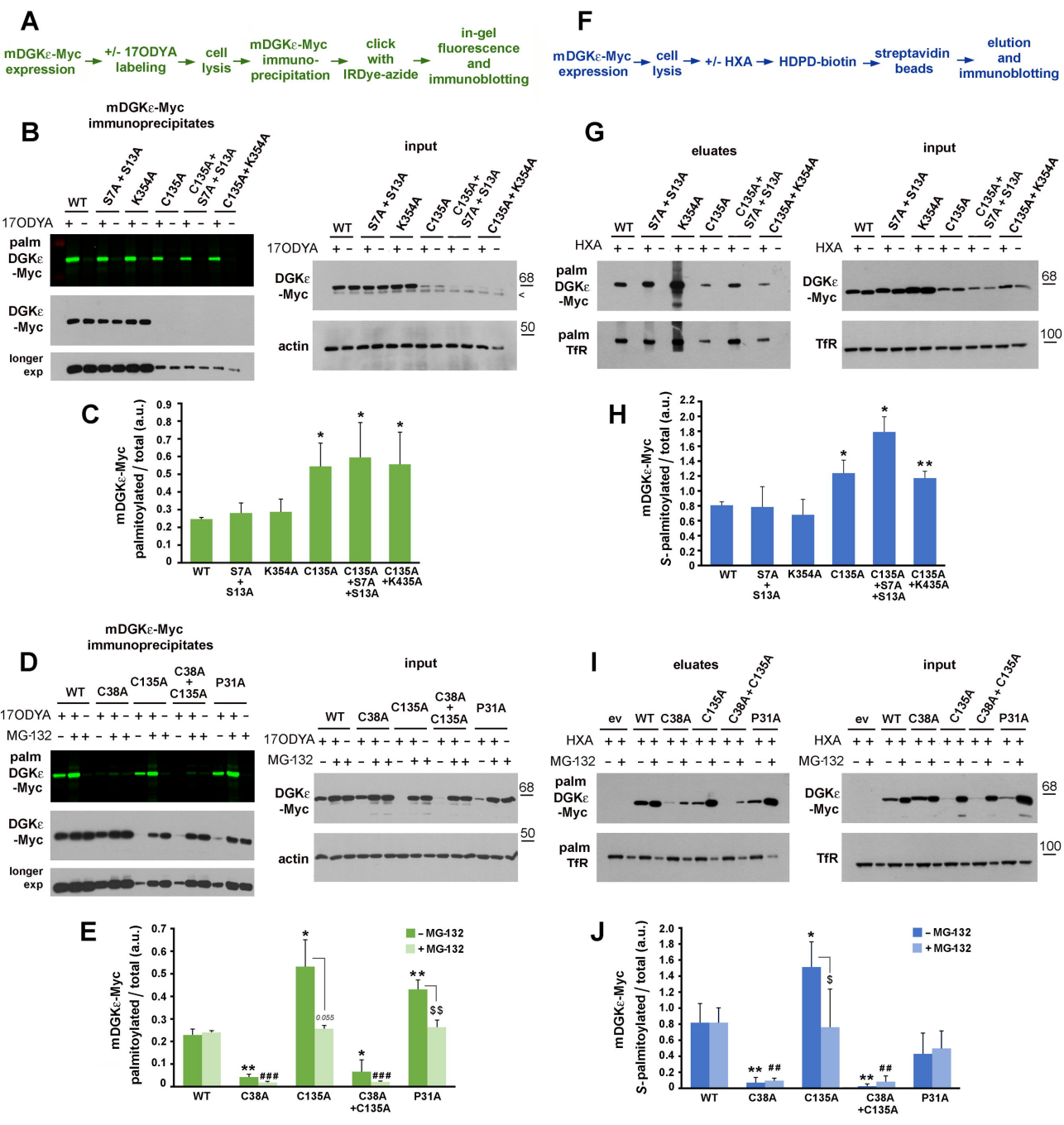
A
mDGKε-Myc expression
+/- 17ODYA labeling
cell lysis
mDGKε-Myc immuno-precipitation
click with IRDye-azide
in-gel fluorescence and immunoblotting
F
mDGKε-Myc expression
cell lysis
+/- HXA
HDPD-biotin
streptavidin beads
elution and immunoblotting
B
mDGKε-Myc immunoprecipitates
WT
S7A + S13A
K354A
C135A
C135A+ S7A + S13A
C135A+K354A
17ODYA
palm DGKε -Myc
DGKε -Myc
longer exp
input
actin
68
50
G
eluates
input
HXA
palm DGKε -Myc
palm TfR
TfR
100
C
mDGKε-Myc palmitoylated / total (a.u.)
WT
S7A + S13A
K354A
C135A
C135A +S7A +S13A
C135A +K435A
H
S-palmitoylated / total (a.u.)
D
mDGKε-Myc immunoprecipitates
C38A
C38A + C135A
P31A
MG-132
I
ev
E
– MG-132
+ MG-132
0.055
C38A +C135A
J
S-palmitoylated / total (a.u.)

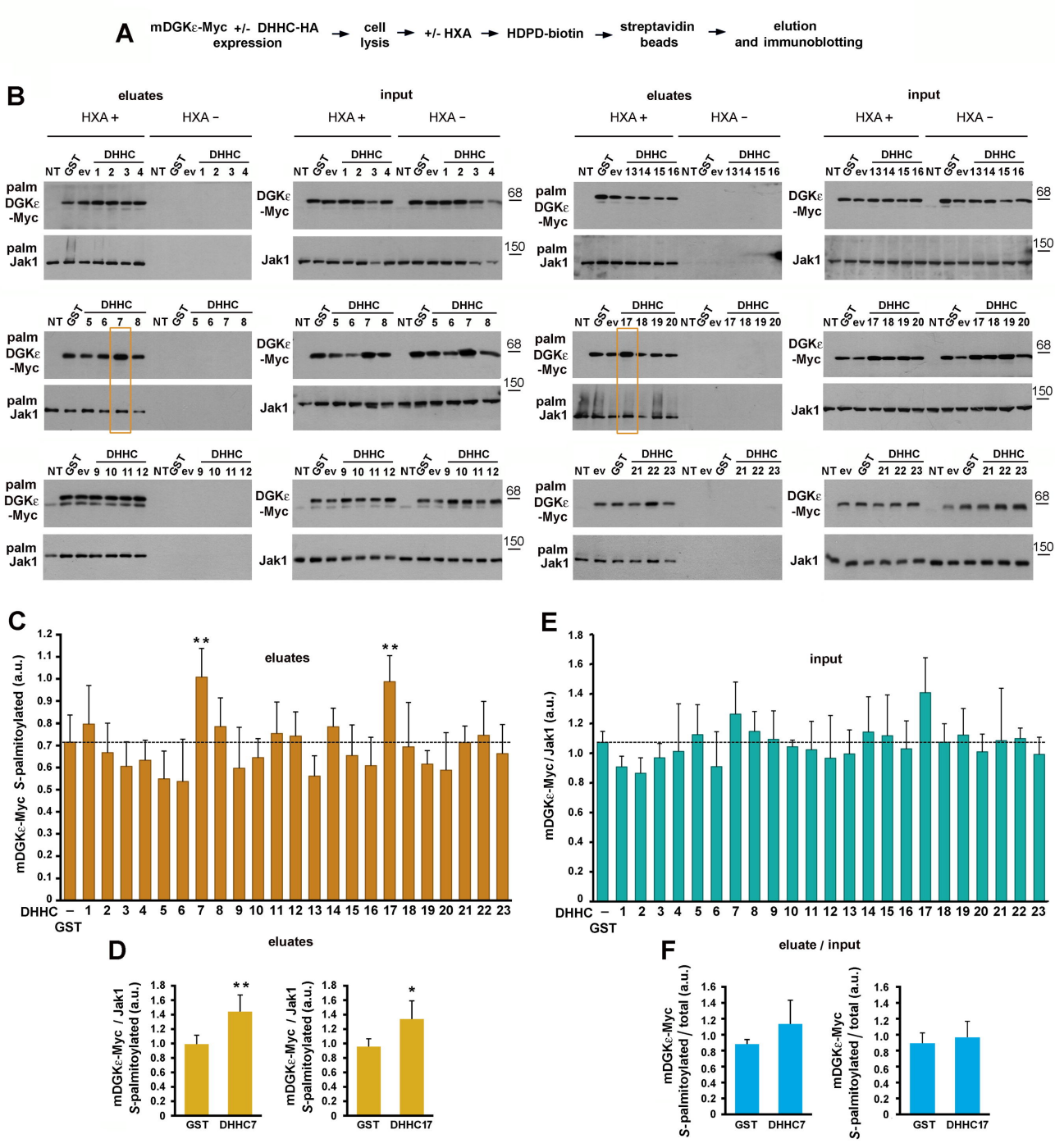
A
mDGKε-Myc +/- expression
DHHC-HA
cell lysis
+/- HXA
HDPD-biotin
streptavidin beads
elution and immunoblotting
B
eluates
input
HXA +
HXA –
palm DGKε -Myc
palm Jak1
DGKε -Myc
Jak1
68
150
C
eluates
mDGKε-Myc S-palmitoylated (a.u.)
DHHC
GST
D
eluates
mDGKε-Myc / Jak1 S-palmitoylated (a.u.)
GST
DHHC7
DHHC17
E
input
mDGKε-Myc / Jak1 (a.u.)
F
eluate / input
mDGKε-Myc S-palmitoylated / total (a.u.)

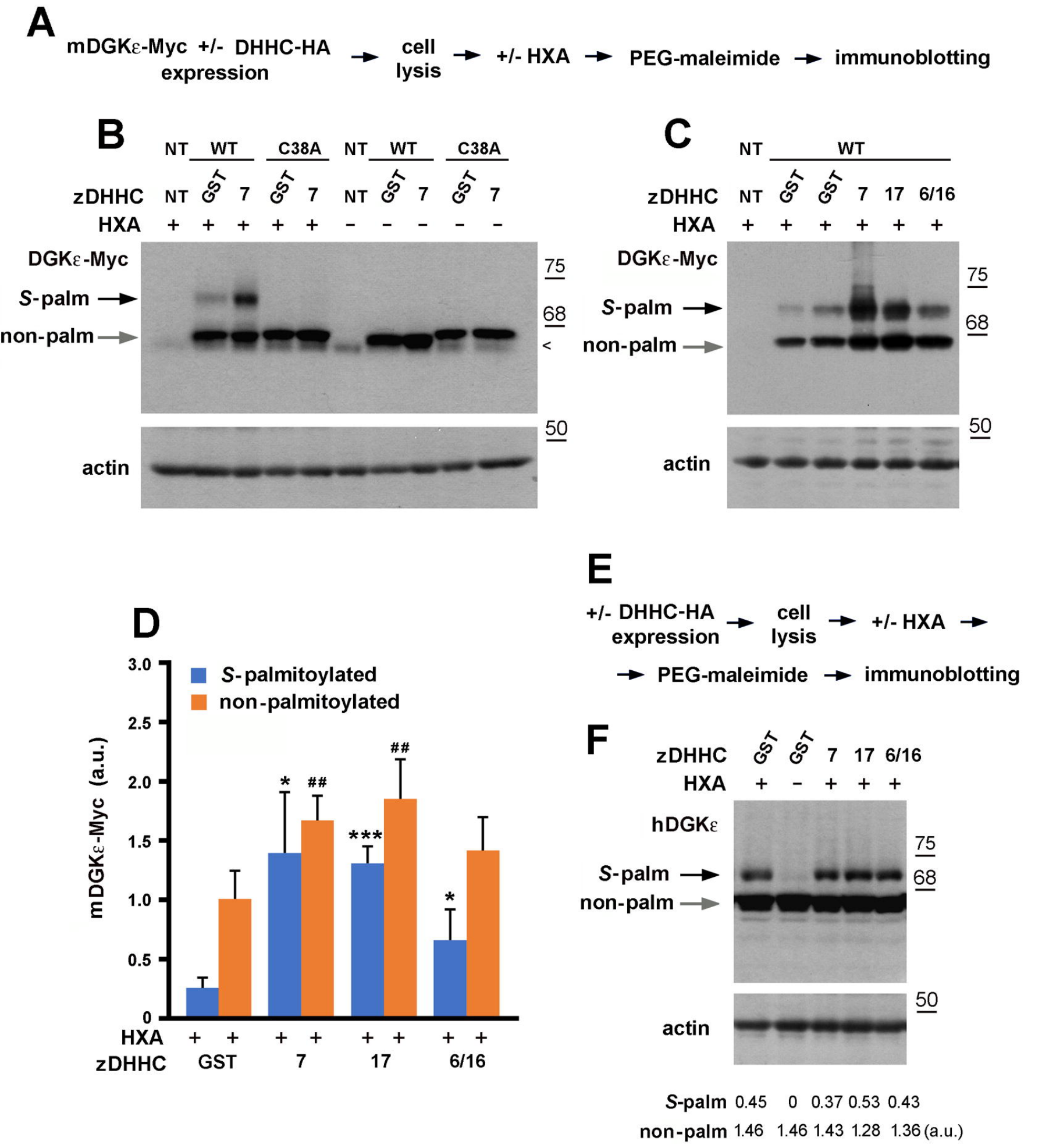
A
mDGKε-Myc +/- DHHC-HA expression
cell lysis
+/- HXA
PEG-maleimide
immunoblotting
B
NT WT C38A NT WT C38A
zDHHC NT GST 7 GST 7 NT GST 7 GST 7
HXA + + + + + − − − − −
DGKε-Myc
S-palm
non-palm
75
68
<
50
actin
C
NT WT
zDHHC NT GST GST 7 17 6/16
HXA + + + + + +
DGKε-Myc
S-palm
non-palm
75
68
50
actin
D
S-palmitoylated
non-palmitoylated
mDGKε-Myc (a.u.)
3.0
2.5
2.0
1.5
1.0
0.5
0
*
##
***
##
*
HXA + + + + + + + +
zDHHC GST 7 17 6/16
E
+/- DHHC-HA expression
cell lysis
+/- HXA
PEG-maleimide
immunoblotting
F
zDHHC GST GST 7 17 6/16
HXA + − + + +
hDGKε
S-palm
non-palm
75
68
50
actin
S-palm 0.45 0 0.37 0.53 0.43
non-palm 1.46 1.46 1.43 1.28 1.36 (a.u.)

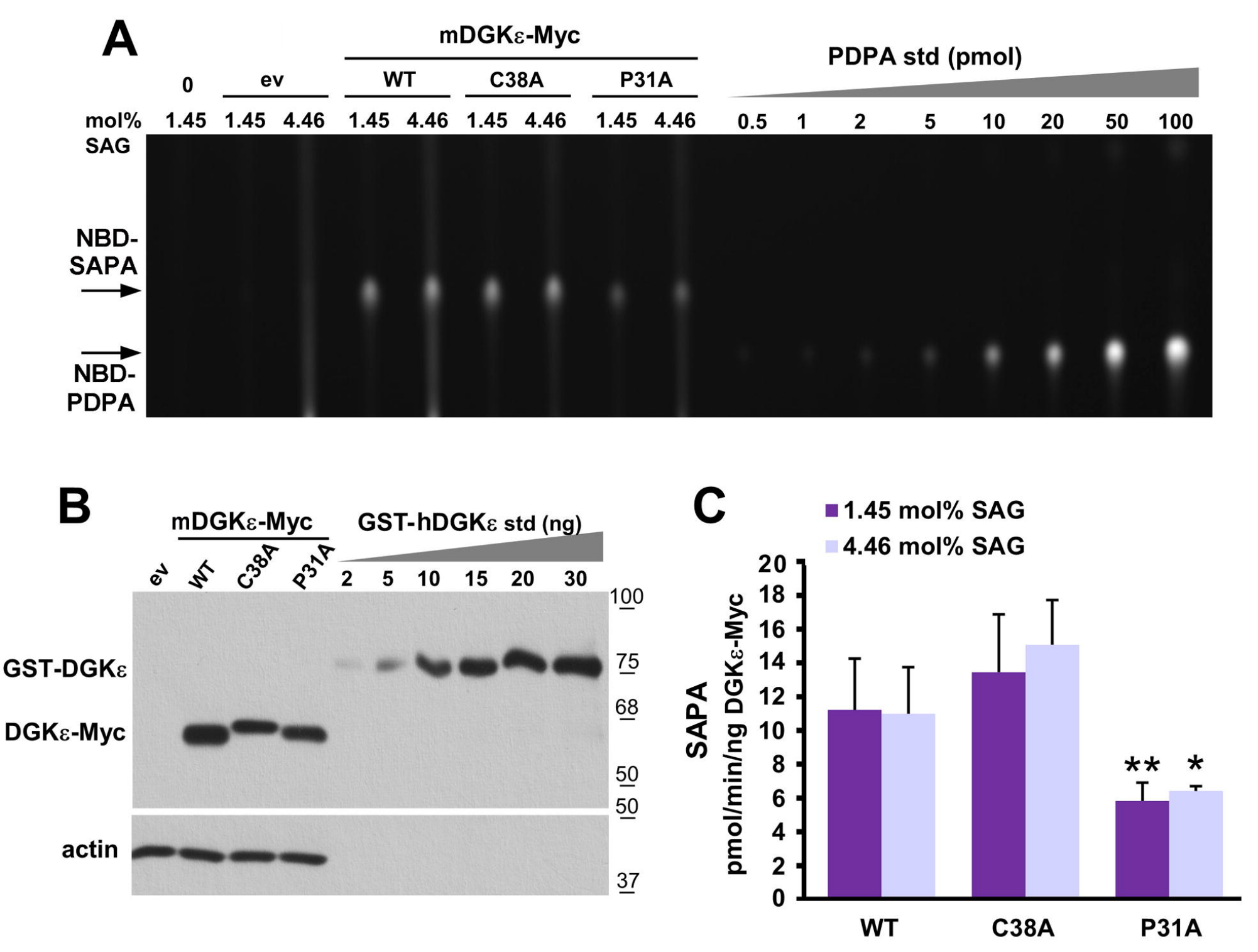
A
mDGKε-Myc
0
ev
WT
C38A
P31A
PDPA std (pmol)
mol% SAG
1.45
1.45
4.46
1.45
4.46
1.45
4.46
1.45
4.46
0.5
1
2
5
10
20
50
100
NBD-SAPA
NBD-PDPA
B
mDGKε-Myc
GST-hDGKε std (ng)
ev
WT
C38A
P31A
2
5
10
15
20
30
GST-DGKε
DGKε-Myc
actin
100
75
68
50
50
37
C
1.45 mol% SAG
4.46 mol% SAG
SAPA
pmol/min/ng DGKε-Myc
20
18
16
14
12
10
8
6
4
2
0
**
*
WT
C38A
P31A